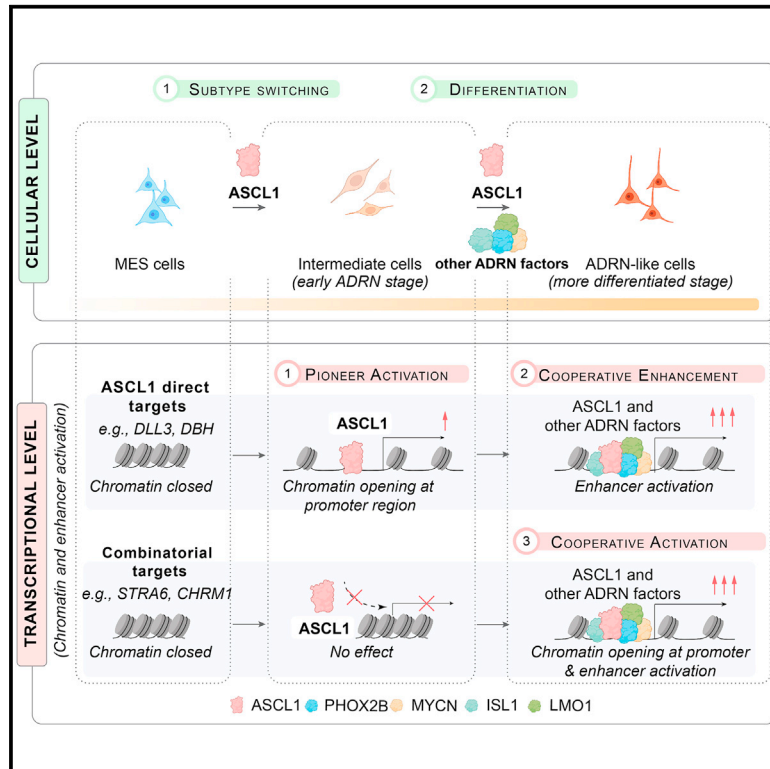


## ASCL1 characterizes adrenergic neuroblastoma via its pioneer function and cooperation with core regulatory circuit factors

### Graphical abstract



### Authors

Lu Wang, Tze King Tan, Hyoju Kim, Dennis Kappei, Shi Hao Tan, A. Thomas Look, Takaomi Sanda

### Correspondence

takaomi\_sanda@u.nus.edu

### In brief

Wang et al. demonstrate that ASCL1 initiated phenotypic changes toward ADRN lineage by altering the chromatin landscape via pioneer factor function in neuroblastoma cells. The authors further show that ASCL1 collaborated with other CRC members during induction and maintenance of specific cellular state.

### Highlights

- ASCL1 functions as a pioneer factor that can alter the chromatin state
- ASCL1 initiates ADRN gene expression program in MES neuroblastoma
- ASCL1 potentiates the activities of other members of CRC
- ASCL1 forms a complex with TCF12 and activates the BMP-SMAD1-ID3/4 pathway



## Article

# ASCL1 characterizes adrenergic neuroblastoma via its pioneer function and cooperation with core regulatory circuit factors

Lu Wang,<sup>1</sup> Tze King Tan,<sup>1</sup> Hyoju Kim,<sup>1</sup> Dennis Kappei,<sup>1,2,3</sup> Shi Hao Tan,<sup>1</sup> A. Thomas Look,<sup>4,5</sup> and Takaomi Sanda<sup>1,3,6,7,\*</sup><sup>1</sup>Cancer Science Institute of Singapore, Singapore 117599, Singapore<sup>2</sup>Department of Biochemistry, Yong Loo Lin School of Medicine, National University of Singapore, Singapore 117596, Singapore<sup>3</sup>NUS Center for Cancer Research, Yong Loo Lin School of Medicine, National University of Singapore, Singapore, Singapore<sup>4</sup>Department of Pediatric Oncology, Dana-Farber Cancer Institute, Harvard Medical School, Boston, MA 02216, USA<sup>5</sup>Division of Pediatric Hematology/Oncology, Boston Children's Hospital, Boston, MA 02215, USA<sup>6</sup>Department of Medicine, Yong Loo Lin School of Medicine, National University of Singapore, Singapore 117599, Singapore<sup>7</sup>Lead contact\*Correspondence: [takaomi\\_sanda@u.nus.edu](mailto:takaomi_sanda@u.nus.edu)<https://doi.org/10.1016/j.celrep.2023.113541>

## SUMMARY

Neuroblastoma originates from developing neural crest and can interconvert between the mesenchymal (MES) and adrenergic (ADRN) states, each of which are controlled by different sets of transcription factors forming the core regulatory circuit (CRC). However, the roles of CRC factors in induction and maintenance of specific state are poorly understood. Here, we demonstrate that overexpression of ASCL1, an ADRN CRC factor, in MES neuroblastoma cells opens closed chromatin at the promoters of key ADRN genes, accompanied by epigenetic activation and establishment of enhancer-promoter interactions, initiating the ADRN gene expression program. ASCL1 inhibits the transforming growth factor  $\beta$ -SMAD2/3 pathway but activates the bone morphogenetic protein SMAD1-ID3/4 pathway. ASCL1 and other CRC members potentiate each other's activity, increasing the expression of the original targets and inducing a new set of genes, thereby fully inducing the ADRN program. Our results demonstrate that ASCL1 serves as a pioneer factor and cooperates with CRC factors to characterize the ADRN gene expression program.

## INTRODUCTION

Neuroblastoma is an embryonic malignancy that originates from early nerve cells and develops in the sympathetic nervous system, with most tumors found in the adrenal medulla. The latest studies revealed more precisely the origin of neuroblastoma to be Schwann cell precursors, which will become bridging cells that differentiate into either adreno-sympathoblasts or chromaffin cells.<sup>1,2</sup> Recent studies classified neuroblastoma into mesenchymal (MES) and adrenergic (ADRN) subtypes, which are associated with the early neural crest and the committed ADRN neural progenitor stages, respectively.<sup>3,4</sup> Interestingly, the MES and ADRN subtypes are interconvertible, demonstrating the plasticity of neuroblastoma.<sup>3–6</sup>

Notably, each of the two neuroblastoma subtypes is controlled by a different set of transcription factors (TFs) that govern a distinct transcriptional program via the formation of an autoregulatory loop called the core regulatory circuit (CRC). Previous studies identified the CRC TFs specific for the MES subtype, such as AP-1 and JUN family TFs, as well as those specific for the ADRN subtype, such as LMO1, ISL1, PHOX2B, GATA3, TBX2, HAND2, and ASCL1.<sup>3,4,7</sup> We previously identified ASCL1 as an integral member of the ADRN CRC that is required for

cell growth and differentiation arrest.<sup>7</sup> ASCL1 encodes a basic-helix-loop-helix (bHLH) TF and plays essential roles in normal neural cell commitment and differentiation. *Asc1* knockout mice show impaired peripheral sympathetic nervous system development.<sup>8</sup> High ASCL1 expression is observed in the bridging cell population.<sup>1,2,9,10</sup> ASCL1 also induces pan-neuronal properties in the reprogramming setting: various types of neuron cells can be generated by different combination of ASCL1 and TFs,<sup>11,12</sup> indicating that ASCL1 serves as a lineage definer. Importantly, ASCL1 can function as a pioneer factor and alter the chromatin structure from the closed to the open state.<sup>13–16</sup> However, functional roles of ASCL1 and cooperative mechanisms with other CRC members in neuroblastoma pathogenesis are poorly understood.

Here, we demonstrate that ASCL1 plays a dominant role to initiate the ADRN gene expression program, accompanied by a dramatic change in the transcriptional landscape and genome-wide epigenetic remodeling in MES neuroblastoma cells. ASCL1 represses the MES gene signature, but activates the ADRN gene signature via regulation of various signaling pathways and cooperation with other ADRN CRC members. ASCL1 is essential for the maintenance of ADRN state of neuroblastoma cells.



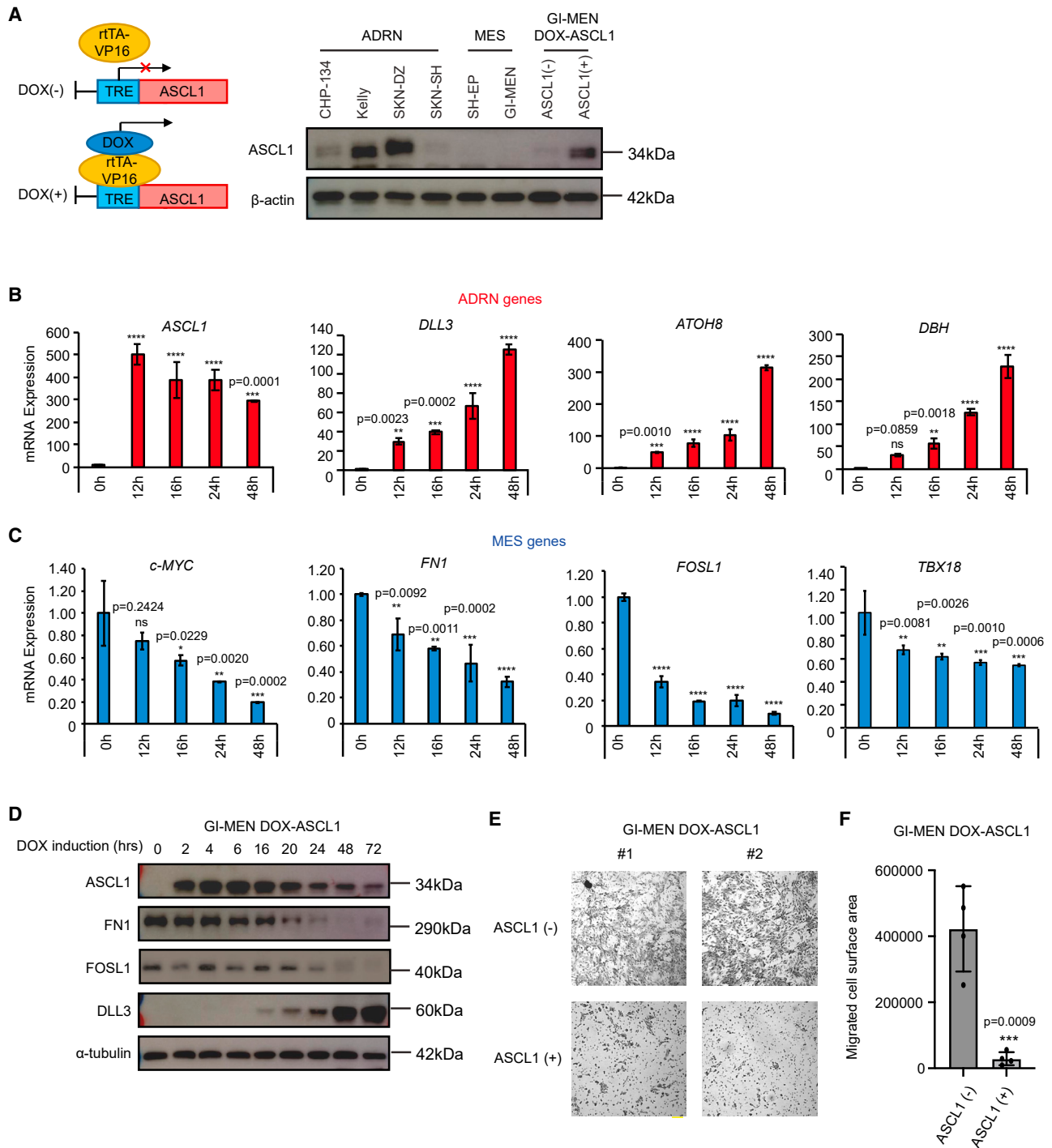


**Figure 1. ASCL1 overexpression in MES cells initiates the ADRN gene expression program**

(A) (Left) A DOX-inducible ASCL1 expression construct was transduced into GI-MEN neuroblastoma cells. (Right) Western blot analysis of different neuroblastoma cell lines and GI-MEN DOX-ASCL1 cells.

(B and C) The mRNA expression levels of ASCL1, ADRN genes (B) and MES genes (C) after DOX induction at different time-points by qRT-PCR. Expression was normalized to GAPDH and is shown as the FC relative to control samples: mean  $\pm$  SD of triplicate samples.

(D) Western blot analysis of GI-MEN DOX-ASCL1 cells after DOX treatment for different time points.

(legend continued on next page)

## RESULTS

### ASCL1 initiates the ADRN gene expression program in MES neuroblastoma cells

In our previous study, we identified ASCL1 as a CRC TF in ADRN neuroblastoma. ASCL1 is specifically expressed in ADRN subtype and not in MES subtype cell lines (Figure 1A). Given its roles in normal development and cell reprogramming, we hypothesized that ASCL1 could be the dominant TF initiating the ADRN-specific gene expression program. To test this hypothesis, we first analyzed phenotypic changes in MES neuroblastoma cells after overexpression of ASCL1 using a doxycycline (DOX)-inducible system. We used two representative MES cell lines (GI-MEN and SH-EP) without baseline expression of ASCL1. Upon DOX treatment, ASCL1 expression was stably maintained in these MES cell lines at a level comparable with that in ASCL1-positive ADRN cell lines (Figures 1A and S1A). We confirmed that the overexpressed ASCL1 was localized mainly in the nucleus in GI-MEN cells. The same pattern was observed for the endogenous ASCL1 protein in the ADRN cell lines (Figures S1B and S1C).

We then investigated whether overexpression of ASCL1 affects the differentiation status of MES cells. We analyzed the expression of several marker genes specific for either the ADRN or the MES state that were selected based on expression patterns in normal neural cells and neuroblastoma cell lines (Figures S1D–S1F). Notably, we observed rapid upregulation of ADRN marker genes such as *DLL3*, *ATOH8*, and *DBH*, while the expression of MES marker genes such as *FN1*, *FOSL1*, and *TBX18* was downregulated in GI-MEN cells after ASCL1 expression (Figures 1B–1D). *c-MYC* (*MYC*), which is expressed in most MES neuroblastoma cells,<sup>3,17</sup> was also downregulated upon ASCL1 overexpression in GI-MEN cells. Similar changes in marker gene expression were also observed in SH-EP cells after ASCL1 expression (Figure S1G). Consistent with the loss of MES features, the migration ability of GI-MEN cells with ASCL1 overexpression was profoundly impaired (Figures 1E and 1F). These results demonstrate that the overexpression of ASCL1 can initiate phenotypic changes in the migratory MES cells toward the ADRN lineage.

### ASCL1 functions as a pioneer factor that opens closed chromatin at key ADRN genes

We next investigated the molecular mechanism by which ASCL1 initiates gene expression programs at the chromatin and epigenetic levels. We first performed chromatin immunoprecipitation sequencing (ChIP-seq) analysis to detect all regions newly bound by ASCL1 in GI-MEN cells. As expected, the ASCL1-bound regions were significantly enriched for the canonical ASCL1/E-box DNA binding motif (Figure 2A).

We then compared the chromatin and epigenetic statuses at ASCL1-bound regions between ASCL1-induced and uninduced conditions using the assay for transposase-accessible

chromatin–sequencing (ATAC-seq) and H3K27ac ChIP-seq. Via these methods, a total of 4,854 differentially opened ATAC peaks (fold-change [FC] of  $>|1.5|$ , adjusted p value  $< 0.05$ ) were identified, which included the peaks that were gained (newly opened), increased, lost (completely closed) or decreased (Figure 2B, top, and Table S1). Notably, nearly 85.83% of gained/increased peaks with ATAC signal were bound by ASCL1. Consistent with the ATAC-seq results, ASCL1 binding was observed at nearly 82.30% of the H3K27ac peaks with gained/increased signals but was rarely observed at the H3K27ac peaks with lost/decreased signals (Figure 2B, bottom). This pattern indicates that ASCL1 binding is associated with chromatin opening and epigenetic activation.

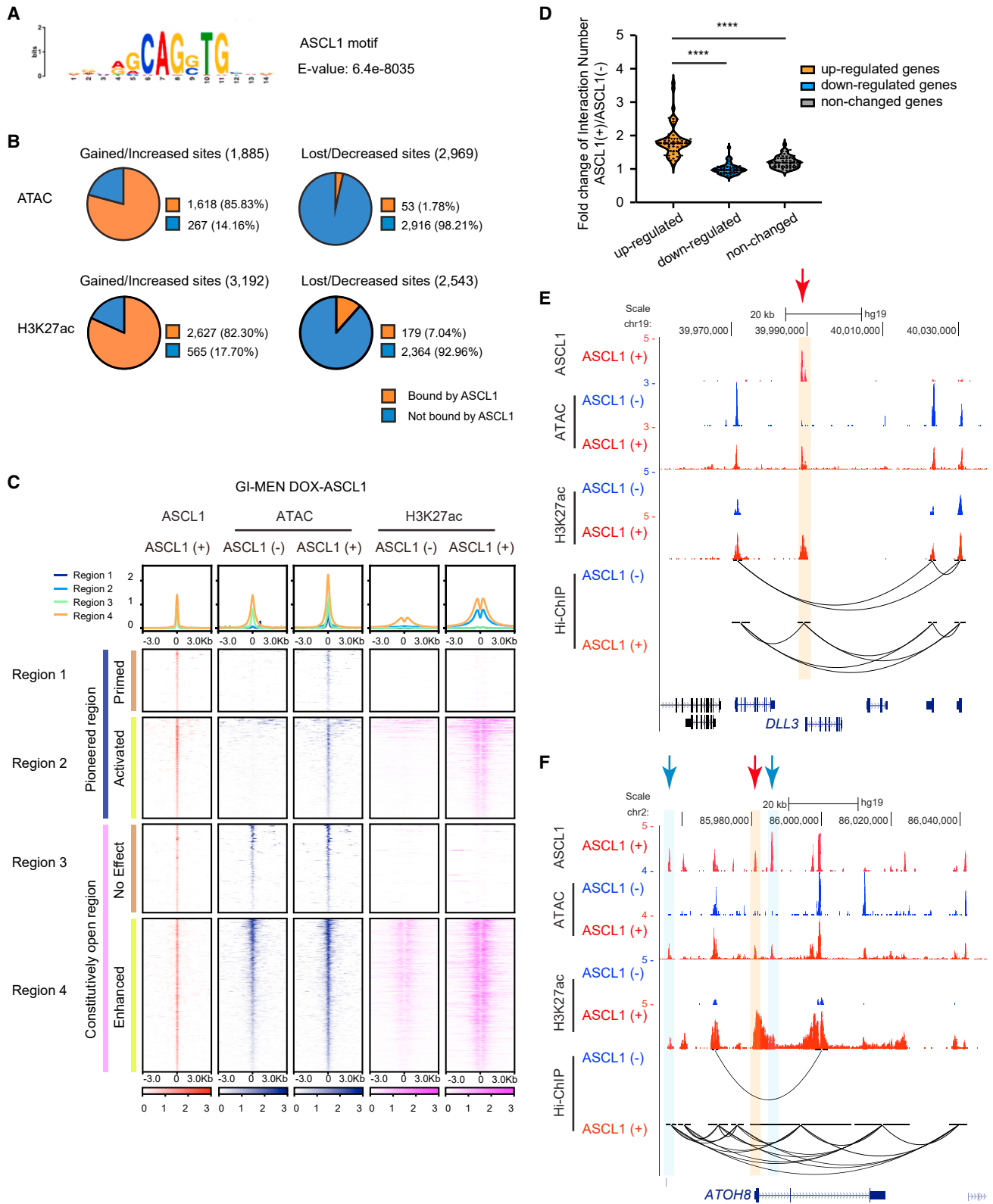
We then classified all ASCL1-bound regions into four groups based on the ATAC-seq and H3K27ac status (Figure 2C). We first focused on the “pioneered” regions (Regions 1 and 2), at which ATAC-seq peaks were gained after ASCL1 overexpression [“ASCL1 (+)"]. Region 1 lacked H3K27ac signals, representing regions that can be opened by ASCL1, but that are not yet epigenetically activated (“primed”). Region 2 contained both gained ATAC-seq signals and H3K27ac signals, representing regions that can be both opened and fully activated by ASCL1 (“activated”). In contrast, regions 3 and 4 contained ATAC-seq peaks regardless of ASCL1 overexpression, indicating that these regions are constitutively open. ASCL1 overexpression did not affect the H3K27ac signals in region 3, representing regions that cannot be activated by ASCL1 (“no effect”). In contrast, region 4 showed stronger H3K27ac signals after ASCL1 overexpression, representing regions that can be further activated by ASCL1 (“enhanced”). We used this classification scheme for the rest of this study.

### Pioneered regions acquire new chromatin-chromatin interactions

We then investigated whether pioneered, activated chromatin regions (represented by region 2) serve as enhancers or promoters. We first categorized genes into three groups: (1) genes whose expression was upregulated by ASCL1, (2) genes whose expression was downregulated by ASCL1, and (3) genes whose expression remained unchanged. The upregulated and downregulated groups comprised the top 50 genes with the highest and lowest FC values, respectively, while the genes in the not changed” group were those with a minimum FC (Table S2) (ranked by  $\log_2$ FC, base mean of  $>100$ , adjusted p value  $< 0.05$ ). We then analyzed chromatin-chromatin interactions via Hi-C chromatin immunoprecipitation (Hi-ChIP) analysis using an anti-H3K27ac antibody. As expected, the upregulated gene group showed the largest increase in the number of chromatin interactions after ASCL1 overexpression (Figures 2D and S2A–S2C). This result suggests a specific effect of ASCL1 on chromatin at the loci of genes upregulated by ASCL1. The gained

(E) Transwell migration assay of GI-MEN DOX-ASCL1 cells treated with DMSO or DOX for 48 h prior to seeding. Representative images were acquired at 40 $\times$  original magnification. Cells were stained with crystal violet. Scale bar, 100  $\mu$ m.

(F) Quantification of the Transwell migration assay was performed using ImageJ to measure the surface area of the Transwell insert covered by migrated cells. Four different images were quantified for each condition. Data are represented as means  $\pm$  SD. The p values by unpaired t test are indicated. (B) and (C) were analyzed by one-way ANOVA followed by Tukey’s multiple comparisons post hoc test. The p values are indicated. \*p  $< 0.05$ . \*\*p  $< 0.01$ . and \*\*\*p  $< 0.001$ . \*\*\*\*p  $< 0.0001$ . ns, not significant.



(legend on next page)

interactions are specific to ASCL1 target genes and are not indicative of an overall effect.

As representative examples for genes from region 2, the *DLL3* and *ATOH8* genes were activated upon ASCL1 overexpression (Figures 1B, 2E, and 2F). Newly opened ATAC peaks as well as enrichment of H3K27ac peaks were observed at their promoters (red arrows) and potential enhancers (blue arrows) bound by ASCL1 in ASCL1-induced GI-MEN cells. The same results were also observed in SH-EP cells (Figure S2D). Consistently, Hi-ChIP demonstrated newly acquired chromatin-chromatin interactions between the promoters and neighboring H3K27ac peaks in ASCL1-induced GI-MEN cells. Together, these data confirm that ASCL1-induced chromatin opening and epigenetic activation lead to the establishment of new chromatin-chromatin interactions and subsequent transcriptional activation.

### ASCL1 can initiate the ADRN gene expression program in MES neuroblastoma cells but is insufficient for complete conversion to the ADRN subtype

To investigate how ASCL1 affects the lineage status of GI-MEN cells, we first analyzed RNA sequencing (RNA-seq) data across a panel of ADRN and MES neuroblastoma cell lines and defined 1,933 MES signature genes and 1,424 ADRN signature genes. Notably, 33.4% of the MES signature genes were downregulated, and 17.8% of the ADRN signature genes were upregulated by ASCL1 overexpression (adjusted p value < 0.05,  $\log_2FC < -0.5$  for downregulation or  $>0.5$  for upregulation) (Figure 3A and Table S3). Thus, ASCL1 can initiate gene expression changes in MES neuroblastoma cells.

Gene set enrichment analysis (GSEA) demonstrated that gene sets, including “E2F targets,” “MYC targets,” and “epithelial-MES transition,” were downregulated upon ASCL1 overexpression. Gene sets known to be involved in neuronal development, such as the transforming growth factor  $\beta$  (TGF- $\beta$ ) (bone morphogenetic protein [BMP]-SMAD1) and WNT- $\beta$ -catenin pathways,<sup>18,19</sup> were upregulated upon ASCL1 overexpression (Figures 3B, S3A, and S3B). Consistent with a previous study,<sup>20</sup> ASCL1 induced genes involved in myocyte lineage (Figure S3B). These results suggest that ASCL1 affects neural differentiation status via transcriptional regulation. Next, we investigated the changes in previously identified ADRN CRC gene expression in GI-MEN cells upon ASCL1 overexpression and found that the mRNA expression

of ADRN CRC genes was still undetectable (i.e., *LMO1*, *PHOX2B*) or unchanged (i.e., *ISL1*, *GATA3*, *TBX2*, *HAND2*) (Figures 3C and S3C). Moreover, it is noteworthy that ASCL1 failed to inhibit the expression of key MES TFs, such as SOX9 (Figure 3A and Table S3). Thus, although overexpression of ASCL1 can initiate gene expression changes, it either does not allow the production of the complete set of ADRN CRC members or is still insufficient to fully convert the gene expression program from MES to ADRN.

### The function of ASCL1 is potentially associated with promoter binding

Therefore, we focused on the genes that are typically expressed in ADRN neuroblastoma cells but cannot be induced by ASCL1 expression in GI-MEN cells. To this end, we compared the ASCL1 and H3K27ac ChIP-seq profiles between GI-MEN cells and a representative ADRN neuroblastoma cell line (Kelly). We selected ASCL1-bound regions in Kelly and divided them into two subregions based on the binding of ASCL1 in ASCL1-induced GI-MEN cells (Figure 3D). Geneset-1 represents loci bound by ASCL1 and associated with high level of H3K27ac signals in both ASCL1-induced GI-MEN cells and Kelly cells. Thus, these regions can be both activated by ASCL1 alone and maintained in ADRN neuroblastoma cells (i.e., *DLL3* and *DBH* loci) (Table S4). In contrast, Geneset-2 represents loci bound by ASCL1 and associated with H3K27ac signals only in Kelly cells and not in ASCL1-induced GI-MEN cells. Although these regions are activated by ASCL1 in ADRN cells at steady state, ASCL1 cannot bind or activate these regions when expressed alone in GI-MEN cells (i.e., *FAM163B*, *CHRM1*, and *TH* loci) (Table S4).

We then investigated the difference in the ASCL1-bound regions between the two groups. DNA motif analysis for each group of ASCL1-bound regions revealed that the canonical ASCL1/E-box motif was the most enriched in both groups (Figure S3D). However, interestingly, ASCL1 binding was more frequently observed at promoters than at enhancers in Geneset 1 regions (Figure 3E), for example, the *DLL3* gene locus shown earlier (Figure 2E). In contrast, more than 75% of the ASCL1 binding events in Geneset-2 regions were at enhancers. Although further evidence is needed, this result suggests that ASCL1 can act as a pioneer factor when it binds to promoters and, thus, can directly activate transcription. However, this effect was not seen for many other ASCL1 targets, which indicated

### Figure 2. ASCL1 functions as a pioneer factor and activates target gene expression

(A) Motifs enriched in ASCL1 binding sites by MEME analysis.

(B) Pie charts showing the percentages of gained/increased and lost/decreased H3K27ac and ATAC peaks that were bound by ASCL1.

(C) Heatmaps showing signals at ASCL1-bound regions in GI-MEN ASCL1 cells and the results of different assays: ASCL1 ChIP-seq signals (red, left), ATAC-seq signals (blue, middle), and H3K27ac ChIP-seq signals (pink, right). The ASCL1-bound regions were first selected in GI-MEN ASCL1 cells, which were classified as pioneered regions (blue bar) and constitutively open regions (pink bar) based on the presence of ATAC peaks. The pioneered regions were further subclassified as primed and activated regions based on the H3K27ac status after ASCL1 expression. The constitutively open regions were further subclassified as no effect regions (brown bars) and enhanced regions (green bars). The metagene plots and density plots show the distribution of ASCL1, ATAC, and H3K27ac peaks at the ASCL1-bound regions ( $\pm 3$  kb from the binding sites).

(D) Violin plot of FC of interaction number in ASCL1(+)/ASCL1(-). Interaction reads of genes locus within 200 kb in GI-MEN ASCL1(-) and ASCL1(+) cells were calculated as the interaction number for one specific locus. Top 50 differentially upregulated or downregulated genes in GI-MEN ASCL1 (+) cells were selected for up-regulated group or down-regulated group. Top 50 genes with minimum FC by ASCL1 were selected for non-changed group. Data are represented as means  $\pm$  SD. The p values by unpaired t test are indicated. \*\*\*\*p value < 0.0001.

(E and F) Gene tracks showing ASCL1 and H3K27ac occupancy, ATAC-seq tracks, and Hi-ChIP signals for H3K27ac interactions at the *DLL3* and *ATOH8* gene loci in GI-MEN-DOX(-) and DOX(+) cells. The arrows indicate the regions with gained ATAC peaks in GI-MEN- DOX(+) cells. Red indicates promoters. Blue indicates putative enhancers.

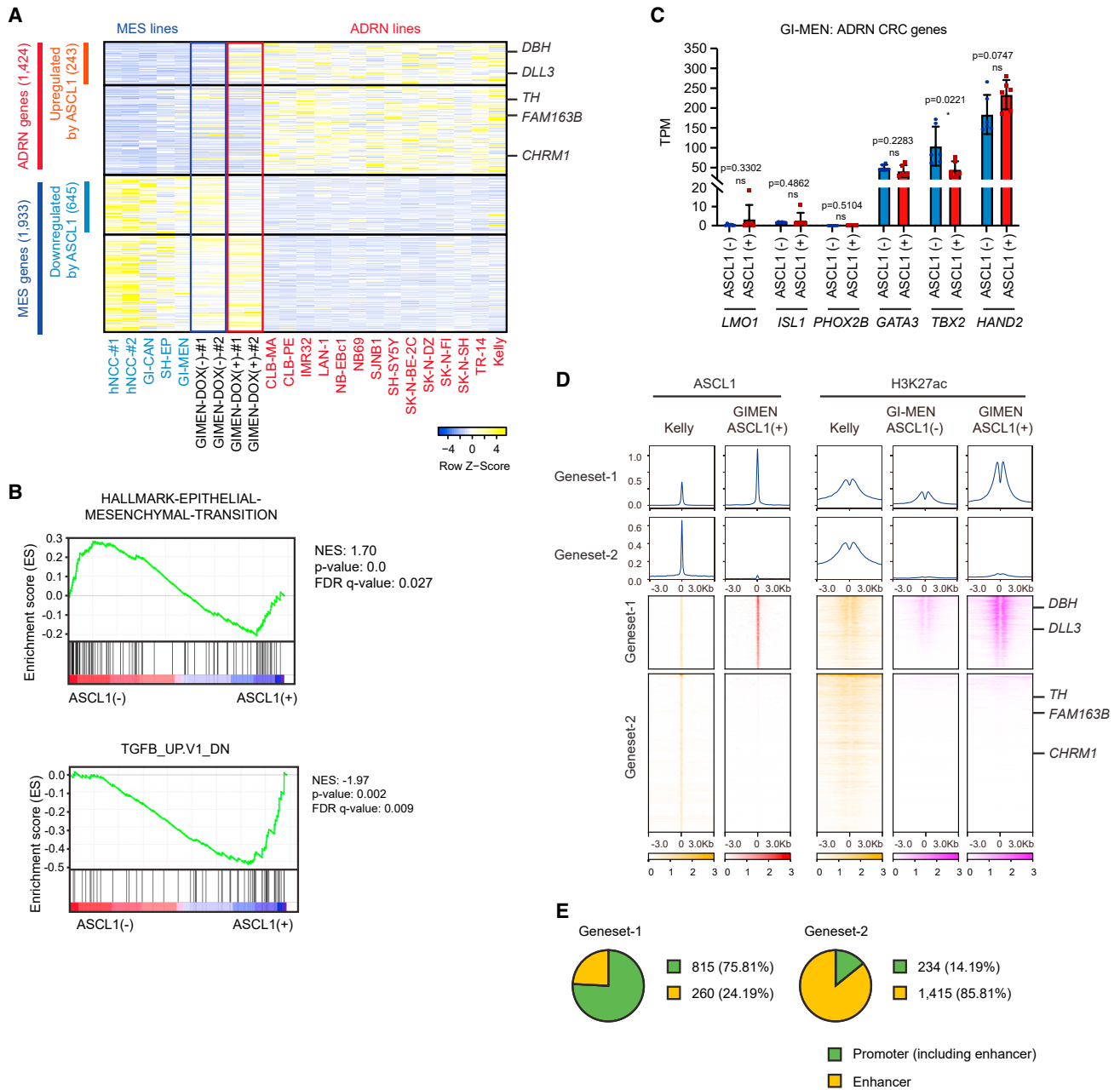


**Figure 3. ASCL1 alone initiates ADNR gene expression program but is insufficient to fully convert the program**

(A) Heatmap analysis of genes that were differentially expressed between ADNR cell lines (dark red) and MES cell lines (dark blue). Subtype-specific genes were defined based on differential gene expression analysis across MES-specific cell lines and ADNR-specific cell lines using public RNA-seq data.<sup>3</sup> FCs were calculated as follows: [average gene expression (TPM) in MES cell lines]/[average gene expression (TPM) in ADNR cell lines]. MES-specific genes and ADNR-specific genes were classified using cutoff values of  $\text{Log}_2\text{FC} = |0.5|$  and an adjusted p value  $< 0.05$ . The final lists of MES-specific genes ( $\text{log}_2\text{FC} < -0.5$ , 1,933 genes) and ADNR-specific genes ( $\text{log}_2\text{FC} > 0.5$ , 1,424 genes) were used to generate the heatmap.

(B) GSEA profile of GI-MEN DOX-ASCL1 cells after DMSO or DOX treatment for 72 h.

(C) mRNA expression levels of the ADNR CRC genes in GI-MEN DOX-ASCL1 cells after 72 h of treatment with DMSO or DOX. Data are represented as means  $\pm$  SD of six biological replicates. (C) was analyzed by multiple unpaired t test. The p values are indicated. \* $p < 0.05$ . Ns, not significant.

(D) ASCL1-bound regions in Kelly cells were classified into two subsets: regions bound by ASCL1 in both Kelly and GI-MEN ASCL1 cells (Geneset-1) and regions specific to GI-MEN ASCL1 cells (Geneset-2). The density plots show the distributions of ASCL1 and H3K27ac signals at the ASCL1-bound regions ( $\pm 3$  kb from the binding sites).

(E) Pie charts showing the proportions of ASCL1-bound enhancers and promoters in Geneset-1 and Geneset-2. Enhancers are all H3K27ac broadPeak that are at least 2,000 bp away from promoters.

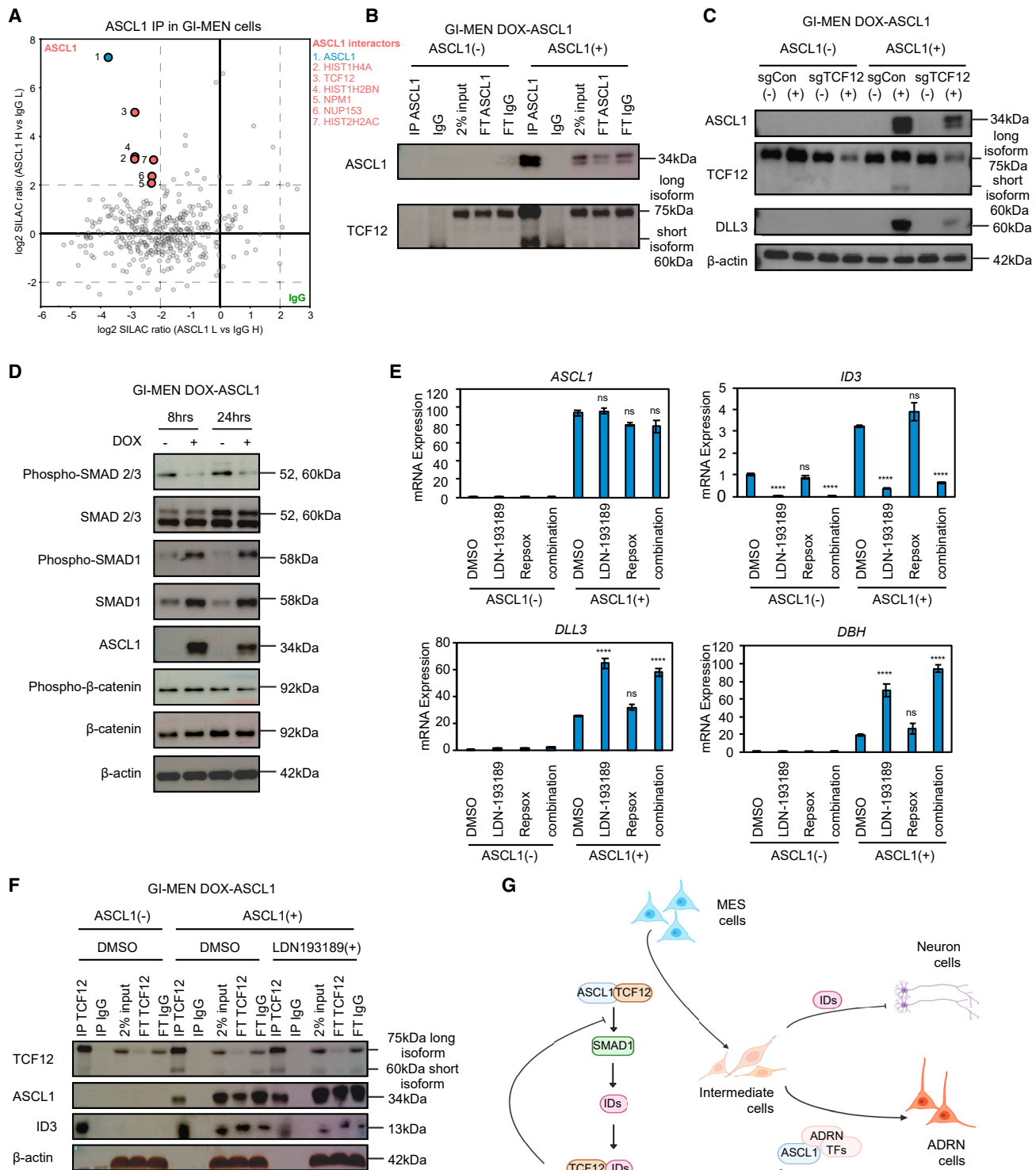


**Figure 4. ASCL1 interacts with TCF12 to activate the SMAD1-ID3/4 pathway, which in turn negatively regulates ASCL1 expression**

(A) Scatterplot of ASCL1 IPs combined with SILAC-based quantitative mass spectrometry in ASCL1-induced GI-MEN cells. Heavy-labeled SILAC extracts were incubated with a ASCL1 antibody and light-labeled extracts with an IgG control (y axis) or vice versa (x axis) and log<sub>2</sub> SILAC ratios are displayed. The ASCL1 bait protein is shown in blue, and other specifically enriched proteins are shown in red.

(legend continued on next page)

that other factors expressed in ADRN neuroblastoma cells were required.

### ASCL1 forms a complex with the E-protein TCF12 to regulate downstream targets

We next analyzed the interacting proteins and signaling pathways that affect the activity of ASCL1. ASCL1 is a class II bHLH TF that forms heterodimers with class I bHLH TFs, including TCF3/E2A, TCF4/E2-2, and TCF12/HEB.<sup>21</sup> However, the interacting proteins of ASCL1 in the context of neuroblastoma are incompletely characterized. Hence, we used the stable isotope labeling by amino acids in cell culture assay to quantitatively detect proteins after IP using an anti-ASCL1 antibody by mass spectrometry analysis (Figure 4A and Table S5). In addition to the bait protein ASCL1, TCF12 was identified as the most strongly enriched hit protein. Notably, ASCL1, TCF3, and TCF4 were pulled down in a reciprocal IP assay using an anti-TCF12 antibody (Figure S4A), consistent with previous findings showing that E-proteins can form hetero- or homodimers.<sup>22</sup> However, in two ADRN cell lines (Kelly and CHP-134), only the TCF12 protein and not the TCF3 or TCF4 protein was detected in the ASCL1 IP eluate (Figure S4B). Interestingly, overexpression of ASCL1 transcriptionally induced the short isoform of TCF12. Validation by individual IP reactions confirmed that both the long and short isoforms of TCF12 were present in the IP eluates (Figures 4B and S4C). Thus, ASCL1-TCF12 is the predominant ASCL1-E-protein dimer formed in ADRN neuroblastoma cells.

To investigate the functional role of TCF12 in ASCL1-mediated transcription, we transduced a DOX-inducible single-guide RNA to specifically knock out either the *TCF12* or *TCF3* gene in GI-MEN cells. Under these conditions, the TCF12 or TCF3 protein was knocked out and ASCL1 was simultaneously overexpressed upon DOX treatment (Figure 4C). Importantly, we observed a strong decrease in DLL3 protein expression by knockout of TCF12 but not TCF3 in the presence of ASCL1 (Figures 4C and S4D). Furthermore, ChIP assay followed by PCR indicated that knockout of TCF12 but not TCF3 reduced the binding of HA-tagged ASCL1 to target gene loci (Figure S4E). Together, these results indicate that TCF12 is the functional partner of ASCL1 that is required for the DNA binding and transcriptional activity of ASCL1, and directly regulates transcription of target genes, such as *DLL3*.

### The BMP-SMAD1-ID3/4 pathway mediates the regulation of ASCL1-TCF12 activity

We next investigated the involvement of signaling pathways when ASCL1 induced ADRN lineage features. We focused on the TGF- $\beta$

and  $\beta$ -catenin pathways, which were enriched in GSEA analysis upon ASCL1 expression in GI-MEN cells (Figures 3B and S3B). We first analyzed the status of surrogate markers for each pathway, including SMAD2/3 (activated by the TGF- $\beta$  pathway), SMAD1 (activated by the BMP pathway), and  $\beta$ -catenin (activated by the WNT pathway). Indeed, upon DOX treatment, significant loss of SMAD2/3 phosphorylation was observed (Figure 4D). In contrast, the level of phosphorylated SMAD1 was increased, accompanied by an increase in the total SMAD1 protein. However, we did not observe any differences in the levels of phosphorylated or total  $\beta$ -catenin after ASCL1 induction (Figure 4D). Of note, SMAD2/3 has been proposed as one of MES CRC members.<sup>4</sup> Thus, overexpression of ASCL1 can repress the MES CRC and shift signaling pathways from MES to ADRN neuroblastoma.

To investigate whether the alteration of these pathways is attributed to the phenotypic change observed after ASCL1 overexpression, we pharmacologically inhibited either the BMP-SMAD1 or TGF- $\beta$ -SMAD2/3 pathway by treatment with LDN-193189 or RepSox, respectively. Each of the inhibitors efficiently inhibited the phosphorylation of SMAD1 and SMAD2/3, respectively (Figure S4F). Interestingly, although LDN-193189 alone was insufficient to induce the expression of ADRN genes such as *DLL3* and *DBH*, it enhanced their expression in the presence of ASCL1 in GI-MEN cells (Figure 4E), indicating that the effect of the BMP pathway depends on ASCL1 expression. In contrast, RepSox treatment did not significantly enhance or inhibit the expression of these mRNAs. This result suggests that activation of the BMP-SMAD1 pathway, but not inhibition of the TGF- $\beta$ -SMAD2/3 pathway, is attributed to the ASCL1-induced conversion to the ADRN subtype.

Of note, ID proteins are known targets of the BMP-SMAD1 pathway.<sup>23–25</sup> Indeed, multiple *ID* genes (*ID1–4*) were significantly upregulated after ASCL1 overexpression in GI-MEN cells (Figure S4G). Independent validation confirmed that ASCL1 overexpression upregulated the mRNA expression of both *ID3* and *ID4*, while this effect was completely abolished by treatment with LDN-193189 (Figures 4E and S4H). Notably, ID proteins bind to E-proteins and sequester them from DNA or type II bHLH TFs (e.g., ASCL1),<sup>26,27</sup> thereby regulating the abundance of functional E-protein dimers. Our results confirmed that TCF12 but not ASCL1 binds to the ID3 protein (Figure S4I). Treatment with LDN-193189, which resulted in a decrease in ID3 expression (compare between the input data in Figure 4F), increased the binding between the ASCL1 and TCF12 proteins (compare between the IP TCF12 data in Figures 4F and S4J). Inhibition of either the BMP-SMAD1 or TGF- $\beta$ -SMAD2/3 pathway did not affect the gene expression

(B) CoIP followed by Western blot analysis of ASCL1 IP in GI-MEN DOX-ASCL1 cells treated with DMSO or DOX for 48 h. IP ASCL1, anti-ASCL1 antibody eluate; IgG, IgG eluate; 2% input, 2% of whole-cell lysate; FT ASCL1, flowthrough with the anti-ASCL1 antibody; FT IgG, flowthrough with IgG.

(C) Western blot analysis of GI-MEN DOX-ASCL1 cells transduced with a single-guide RNA (sgRNA) targeting scrambled sequence or *TCF12* gene. Cells were treated with DMSO or DOX for 48 h.

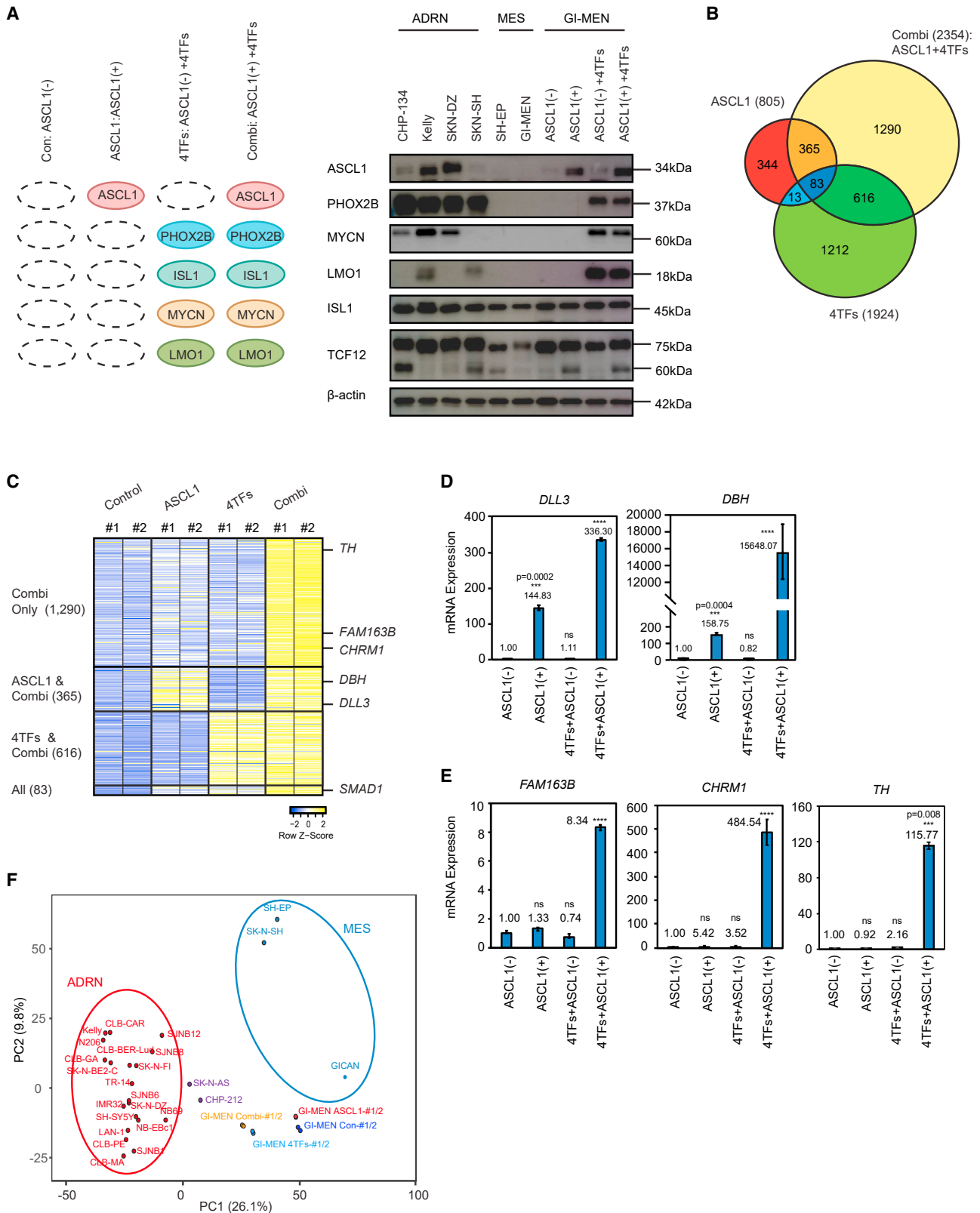
(D) Western blot analysis of GI-MEN DOX-ASCL1 cells after DOX treatment for 48 h.

(E) mRNA expression levels of *ASCL1*, *ID3*, *DLL3*, and *DBH* in GI-MEN DOX-ASCL1 cells after 48 h of treatment with DMSO or DOX and LDN-193189, RepSox, or a combination of both by qRT-PCR. Expression was normalized to *GAPDH* and is shown as the FC relative to control samples: mean  $\pm$  SD of triplicate samples.

(F) CoIP Western blot of TCF12 IP in GI-MEN DOX-ASCL1 cells treated with DMSO, DOX, or DOX and LDN-193189 for 48 h.

(E) Analysis by one-way ANOVA followed by Tukey's multiple comparisons post hoc test. The p values are indicated. \*\*\*\*p value < 0.0001. ns, not significant. See also Figure S3 and Table S2.

(G) A diagram showing the relationships of ASCL1 to BMP signaling and ID proteins.



(legend on next page)

of any CRC member (Figure S4K). Our results suggest that the BMP-SMAD1-ID3/4 axis serves as a mechanism to fine-tune the activity of ASCL1 (Figure 4G).

### Overexpression of other ADRN CRC TFs promotes gene expression changes from the MES to the ADRN neuroblastoma program

Next, we sought to understand why expression of only ASCL1 failed to induce full conversion toward the ADRN lineage. One possible explanation is that other ADRN CRC members need to be expressed together with ASCL1 to fully induce ADRN genes. Thus, we experimentally overexpressed all four components (i.e., MYCN, PHOX2B, ISL1, and LMO1, referred to hereafter as 4TFs) in GI-MEN cells with or without ASCL1 at levels comparable with those in ADRN cell lines (Figure 5A). Because two other ADRN CRC genes, *HAND2* and *GATA3*, are already expressed in GI-MEN cells at baseline (Figures 3C and S5A), we did not further overexpress these genes. Using this system, we performed RNA-seq analysis and selected genes that were upregulated in each of the three comparisons (adjusted p value < 0.05, log2FC > 1, TPM of >1) (Figure 5B): (1) control vs. ASCL1 alone (ASCL1), (2) control vs. 4TFs (4TFs), and (3) control vs. ASCL1 + 4TFs (Combi). Notably, there was a relatively small overlap between the ASCL1 and 4TF conditions. Among the 805 genes that were upregulated by ASCL1 alone, only 11.9% were also upregulated by 4TFs, while most, including key ADRN markers such as *DLL3* and *DBH*, were not affected by 4TFs (Figures 5B and 5C). Conversely, most of the genes that were upregulated by 4TFs were not affected by ASCL1 alone. This result suggests that ASCL1 and 4TFs regulate different sets of genes.

Importantly, the combination of ASCL1 and 4TFs potentiated the expression of the ASCL1 target genes and induced the expression of a new set of genes. Among the 709 genes that were upregulated by ASCL1 alone but not by 4TFs, 365 (51.5%), such as *DLL3*, were further upregulated after the addition of 4TFs (Figures 5B–5D). Most strikingly, a total of 1,290 genes were upregulated only when 4TFs and ASCL1 were co-expressed (Figures 5B–5E and Table S6). These genes included a new set of genes, such as *FAM163B*, *CHRM1*, and *TH* (Figure 5E). *TH* is typically expressed in more differentiated ADRN cells during normal development (Figure S1E). The expression of these genes was increased in a time-dependent manner after ASCL1 induction (Figures S5B and S5C). Notably, cross-comparison with Genesets 1 and 2 from Figure 3D demonstrated that many of these Combi target genes (*FAM163B*, *CHRM1*, and *TH*) were in Geneset 2, which was activated only in the ADRN cell line (Kelly) and not in

ASCL1-induced GI-MEN cells. This pattern further suggested that the other TFs were required to initiate Combi target gene expression. Collectively, the principal component analysis results demonstrated that samples co-expressing ASCL1 and the other CRC members were located closer to ADRN cell lines than were samples expressing ASCL1 or 4TFs (Figure 5F), thus showing that the gene expression signature in 4TFs + ASCL1 cells is more similar to that in the ADRN state. Moreover, when we silenced ASCL1 expression by withdrawing DOX after 12 days of treatment in the presence of 4TFs, the mRNA expression levels of all ASCL1 target genes were reversed to the original levels (Figures S5D–S5G). This result indicates that the expression of the target genes is highly dependent on ASCL1 and cannot be maintained by the other 4TFs.

Pathway analysis with the Enrichr tool demonstrated that the genes activated by ASCL1 alone were related to somitogenesis (Figure S5H), suggesting that ASCL1 activated genes that were enriched in processes related to the early development of neural crest cells. The addition of 4TFs selectively increased the expression of genes related to neuron development but suppressed the expression of nonneuronal genes (mostly related to the myocyte lineage) activated by ASCL1 (Figures S5I and S5J), suggesting that the other 4TFs collaborated with ASCL1 to further specify the neuronal lineage. In contrast, genes activated by 4TFs were enriched in cell-cycle-related pathways (Figures S5I–S5K), suggesting that those genes might contribute to the proliferation feature of neuroblastoma cells. These results indicate that ASCL1 and other ADRN CRC factors regulate different sets of genes that are involved in different cell lineages or stages, and that the combination of these factors can generate a gene expression signature corresponding with more differentiated ADRN cells.

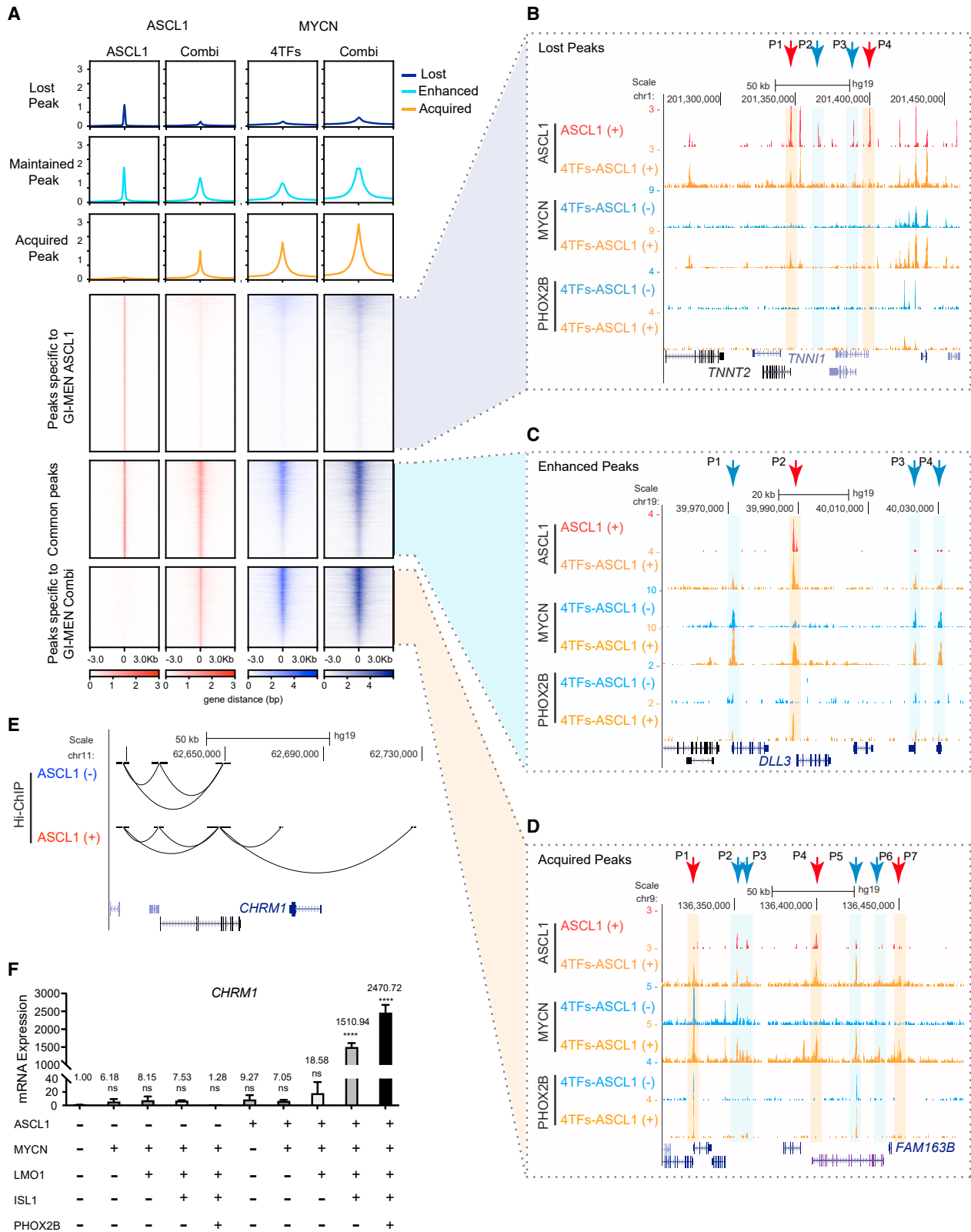
### ASCL1 and other ADRN CRC members reciprocally potentiate their activities

We then investigated the potential mechanisms by which ASCL1 cooperates with 4TFs. To determine the effects of ASCL1 and 4TFs on the DNA binding of each TF and the epigenetic status, we performed ATAC-seq and the cleavage under targets and release using nuclease assays for ASCL1, PHOX2B, MYCN, and H3K27ac in GI-MEN cells under all four different conditions. We first selected all regions bound by ASCL1 and then classified them into three groups of regions (Figure 6A, compare between left two panels).

The first group (top) represents the regions that were bound by ASCL1 only under the ASCL1 condition and not under the Combi

**Figure 5. The addition of 4TFs in combination with ASCL1 activates the expression of new gene subsets**

(A) (Left) The four different conditions. (Right) Western blot analysis of neuroblastoma cell lines, and GI-MEN cells under the four different conditions.  
(B) Venn diagram of genes upregulated under the ASCL1, 4TFs, and Combi (ASCL1 + 4TFs) conditions. Targets were filtered out with the threshold log2FC > 1, adjusted p value < 0.05.  
(C) Heatmap of genes upregulated only under the Combi condition (top), genes upregulated under both the ASCL1 and Combi conditions (second), genes upregulated under both the 4TFs and Combi conditions (third), and genes upregulated under all conditions (bottom).  
(D and E) The mRNA expression of representative gene targets after 48 h of DOX induction by qRT-PCR. Expression was normalized to *GAPDH* and is shown as the FC relative to control samples: mean ± SD of triplicate samples.  
(F) Principal component analysis (PCA) was performed for neuroblastoma cell lines and GI-MEN cells under the four conditions. Blue, red, and purple represent MES, ADRN, and intermediate cell lines, respectively. The dark blue, red, light blue, and light orange dots represent GI-MEN Con, ASCL1, 4TFs, and Combi cells, respectively. (D) and (E) were analyzed by one-way ANOVA followed by Tukey's multiple comparisons post hoc test. The p values are indicated. \*\*\*\*p value < 0.0001. ns, not significant.



(legend on next page)

condition. Thus, these regions lost the binding of ASCL1 when 4TFs were expressed together (lost peaks). For example, loss of ASCL1 binding was observed at the *TNNT2* and *TNNI1* gene loci, and no MYCN or PHOX2B binding was observed at these sites (Figure 6B). These genes are nonneuronal lineage genes (Figures S5E and S5F). Thus, although ASCL1 can regulate these genes, their expression can be suppressed by 4TFs, thereby potentially specifying the neuronal lineage fate.

The second group (middle) represents the regions that were bound by ASCL1 under both the ASCL1 and Combi conditions. We observed similar ASCL1 binding peaks at these regions under the Combi condition and ASCL1 condition. Thus, these regions maintained the peaks upon the addition of 4TFs (maintained peaks). For example, the original peak bound by ASCL1 in ASCL1 condition was still present at *DLL3* gene locus (red arrow, Figure 6C).

The third group (bottom) represents the regions that were bound by ASCL1 only under the Combi condition. Thus, these regions can be bound by ASCL1 only when overexpressed with 4TFs (acquired peaks). For example, newly acquired ASCL1 binding sites were found at the *FAM163B* gene locus as well as enhancer peaks nearby *DLL3* locus (blue arrows, Figures 6C and 6D), demonstrating cooperative activities among the TFs.

### Mechanisms of cooperative activity between ASCL1 and other CRC members

Hence, we finally focused on the maintained and acquired peaks, because these regions should have potential mechanisms underlying the cooperative actions among ASCL1 and 4TFs. Interestingly, ASCL1 affected the DNA binding of the other TFs. Global profiling revealed increased bindings of MYCN at these regions under the Combi condition compared to the 4TFs condition (Figure 6A, compare between right two panels).

As an example, newly acquired binding of MYCN and PHOX2B was observed in the presence of ASCL1 at the promoter of the *DLL3* gene locus (Figure 6C, peak P2), which was associated with the gained H3K27ac signals (Figure S6A, red arrow). Thus, this element is co-occupied by CRC factors and more highly activated under the Combi condition. Similar effects were observed at the *FAM163B* and *CHRM1* gene locus (Figures S6B and S6C, red arrows). These findings indicate that these genes can be pioneered by ASCL1 via promoter binding and further activated via the recruitment of other TFs, explaining the pattern of expression shown in Figures 5D and 5E.

We then focused on the acquired targets (e.g., *TH*, *CHRM1*, and *FAM163B*) and sought to determine why they can be induced when all factors are expressed. Notably, although the expression of these genes could not be induced by ASCL1 overexpression alone, increased chromatin-chromatin interactions were observed at these gene loci after ASCL1 overexpression alone (Figures 6E and S6D). These gene loci also exhibited gained binding of MYCN and H3K27ac signals with the addition of ASCL1 (Figure 6D [see peaks P4–7] and S6B–S6C). Importantly, the gene expression of *CHRM1* could not be induced by any different combinations of the other 4 TFs, but was induced by ASCL1 in combination with at least one other factor, such as PHOX2B or ISL1 (Figure 6F). These results indicate a cooperative action among ASCL1 and the other TFs.

### DISCUSSION

Neuroblastoma cells maintain a high level of plasticity to change their lineage and differentiation status. Recent studies have demonstrated that the MES and ADRN subtypes are interconvertible. ADRN lineage neuroblastoma cells can be dedifferentiated into MES neuroblastoma cells via overexpression of MES-specific CRC genes, such as *PRRX1*<sup>4</sup> or *NOTCH1*.<sup>5</sup> Cell differentiation status can also be changed via activation of the RAS signaling pathway<sup>28</sup> or the removal of epigenetic regulators such as the ARID1A protein.<sup>6</sup>

In this study, we first demonstrated that a single gene expression of ASCL1 can dramatically alter the cellular state by repressing MES-specific genes and activating ADRN-specific genes. This phenomenon is attributed to ASCL1's inherent capacity as a broad lineage definer, which shapes the landscape of ADRN lineage program during normal neural development. ASCL1 is normally expressed in the Schwann cell precursor and bridging cells, preceding the stages at which other ADRN neuroblastoma CRC members (i.e., PHOX2B, ISL1) are expressed. Thus, ASCL1 leads cells to ADRN lineage by initiating the ADRN program, while other TFs further delineate the ADRN lineages.<sup>12</sup> Importantly, when ASCL1 is expressed in GI-MEN cells, it can open closed chromatin and bind to the promoters of key ADRN gene loci as a pioneer factor, such as those of the *DLL3* and *DBH* genes, and rapidly activate transcription. This event leads to the establishment of enhancer-promoter interactions. Furthermore, our study suggests a specific order for TFs to access a particular gene locus. ASCL1 is the initial TF to open closed

### Figure 6. The distribution of ASCL1 is dependent on other TFs, while chromatin-chromatin interactions are established by ASCL1 prior to activation of gene expression

(A) Heatmaps showing signals at ASCL1-bound regions in GI-MEN ASCL1 cells and GI-MEN Combi cells and the results of different assays: ASCL1 cleavage under targets and release using nuclease (CUT&RUN) signals (red, left) and MYCN CUT&RUN signals (blue, right). The regions were classified into three subsets: regions specific to GI-MEN ASCL1 cells (Lost peaks), regions commonly bound by ASCL1 in both GI-MEN ASCL1 cells and GI-MEN Combi cells (Enhanced peaks), and regions specific to GI-MEN Combi cells (Acquired peaks). The metagene plots and density plots show the distributions of ASCL1 and MYCN at the ASCL1-bound regions ( $\pm 3$  kb from the binding sites).

(B–D) Gene tracks of ASCL1 CUT&RUN in GI-MEN-ASCL1(+) and ASCL1(+) +4TFs cells, MYCN and PHOX2B CUT&RUN in GI-MEN-ASCL1(–) + 4TFs and ASCL1(+) +4TFs cells are shown at three gene loci: *TNNT2* (B), *DLL3* (C), and *FAM163B* (D). The arrows indicate lost peaks (B), retained peaks (C), and acquired peaks (D). Red indicates promoters. Blue indicates putative enhancers.

(E) Gene tracks showing H3K27ac Hi-ChIP interactions at the *CHRM1* gene loci in GI-MEN DOX(–) and DOX(+) cells.

(F) The mRNA expression of *CHRM1* in cells expressing different combinations of TFs by qRT-PCR. Cells were treated with DMSO or DOX for 5 days. Expression was normalized to *GAPDH* and is shown as the FC relative to control samples: mean  $\pm$  SD of triplicate samples. (F) was analyzed by one-way ANOVA followed by Tukey's multiple comparisons post hoc test. The p values are indicated. \*\*\*\*p value < 0.0001. ns, not significant.

chromatin, allowing subsequent binding of other TFs, such as PHOX2B and MYCN. Without ASCL1, other factors cannot access the corresponding loci. Consistently, a recent study by Parkinson et al. showed that the loss of ASCL1 in ASCL1-expressing neuroblastoma cells led to changes in chromatin accessibility and affected the binding of GATA3 and PHOX2B.<sup>29</sup> While the ability of ASCL1 to initiate chromatin opening cannot be completely demonstrated by the loss-of-function approach, the results of Parkinson et al. complement our findings that ASCL1 could regulate chromatin accessibility as a pioneer factor.<sup>29</sup> Another study by Woods et al. aligns with our research by showing that overexpression of ASCL1 results in the activation of dopaminergic neuronal genes.<sup>30</sup> Collectively, our findings support the existence of a hierarchical order among the ADRN CRC factors, in which ASCL1 plays a dominant role in initiating and maintaining the ADRN gene expression program.

Importantly, we also found that single ASCL1 is insufficient for complete conversion to the ADRN state. ASCL1-overexpressing GI-MEN cells adopted an intermediate state between the MES and ADRN states that resembles the bridging cell stage between Schwann cell precursor cells and connecting progenitor cells found during normal development. Hence, we consider two potential mechanisms underlying this incomplete conversion. First, ASCL1 could not activate the expression of other ADRN CRC members or a subset of ADRN-specific genes. Second, ASCL1 failed to silence the other subset of MES-specific genes, including SOX9. SOX9 is important for maintaining neural stem cell function. During the physiological neural differentiation process, ASCL1 suppresses SOX gene expression and mitigates the repressive effect of SOX genes on PHOX2A expression, facilitating progenitor cell differentiation. Hence, failure to inhibit SOX gene expression by ASCL1 could be another important factor for incomplete conversion.

Notably, we showed that a full set of CRC members is required for acquisition of the ADRN neuroblastoma identity. This mechanism can be explained by at least four different roles of ASCL1 and other CRC members through which they cooperate for gene regulation (see the [Graphical abstract](#)). First, ASCL1 activates the ADRN gene expression program as a pioneer factor by opening chromatin at the promoters of Geneset-1 genes (e.g., *DLL3*, *DBH*), which initiates phenotypic changes (pioneer activation). This event also allows the binding of other TFs, such as MYCN and PHOX2B, which leads to the second mechanism, enhanced transcriptional activation of downstream target genes (cooperative enhancement) ([Figure 6C](#)). In the third mechanism, other TFs recruit ASCL1 to the gained peak sites and induce a different set of target genes, namely, Geneset-2 genes (e.g., *FAM163B*, *CHRM1*, and *TH*), which are further activated by ASCL1 via its non-pioneer factor function, accomplished through enhancer activation and the establishment of chromatin-chromatin interactions (cooperative activation) ([Figure 6D](#)). In the last mechanism, TFs such as MYCN and PHOX2B regulate the binding sites of ASCL1. Upon introduction of other TFs, ASCL1 occupancy decreased at the lost peak sites, which contained nonneuronal lineage genes ([Figure 6B](#)). This observation suggests that other TFs suppress the activity of ASCL1 toward nonneuronal lineage genes ([Figure S5E](#)). Hence, CRC members play different roles depending on the target locus and cooperate

to fully induce the ADRN signature. Similarly, previous finding have implicated both the pioneer factor and non-pioneer factor functions of ASCL1 in iPSC-derived human neural differentiation. The interaction of ASCL1 with the BAF SWI/SNF chromatin remodeling complexes was found to be more predominant at permissive sites where ASCL1 functions as a non-pioneer remodeling factor. It would be interesting to investigate whether similar chromatin remodelers interact with ASCL1 at the regions where ASCL1 acts as a pioneer factor or as a non-pioneer factor in the neuroblastoma context.

Our study also demonstrated that the ASCL1-driven gene expression program remains reversible, as shown by the withdrawal assay. MES CRC (i.e., SMAD2/3) can be dissolved by ASCL1 overexpression, which allows cells to take on different subtype. Thus, CRC members need to be stably expressed to maintain the steady state of phenotypic state. In the setting of human ADRN neuroblastoma, ASCL1 expression is stably maintained due to genetic mechanisms. LMO1 and MYCN, two major upstream factors of ASCL1, are irreversibly and highly expressed due to a germline polymorphism and genetic amplification, respectively,<sup>31–34</sup> which can induce ASCL1 expression at a high level.<sup>7</sup> This mechanism may be essential to maintain a specific lineage state and ADRN gene expression program via formation of the CRC.

Lineage conversion between two neuroblastoma subtypes contributes to the heterogeneity of neuroblastoma tumors, potentially leading to drug resistance or relapse after chemotherapy. By studying the process of ASCL1-induced lineage conversion from the MES to the ADRN subtype, we could gain a better understanding of the molecular mechanism underlying this phenomenon and potentially overcome drug resistance caused by lineage conversion. Our findings show the mechanism by which ASCL1 induces subtype switching and signaling cascade alterations to convert MES neuroblastoma cells to ADRN neuroblastoma cells. The unique roles of ASCL1 as a pioneer factor and an ADRN CRC member directly contribute to the initiation and maintenance of the oncogenic transcriptional program. This finding provides a more detailed understanding of the molecular pathogenesis of ADRN neuroblastoma.

### Limitation of the study

In this study, we have demonstrated the cooperative relationship between ASCL1 and other TFs during phenotypic conversion of neuroblastoma cells; however, we only examined specific TFs identified in our previous study. Of note, there are additional neural crest pioneer TFs that could be missing pieces for the sympathoadrenal program, such as TFAP2B. TFAP2B is responsible for activating the sympathoadrenal program, operating autonomously from BMP signaling or ASCL1. Furthermore, our study currently used only the *in vitro* system due to technical limitations. Hence, it is important to further analyze whether the same mechanism is observed in animal models and clinical samples.

### STAR★METHODS

Detailed methods are provided in the online version of this paper and include the following:

- **KEY RESOURCES TABLE**
- **RESOURCE AVAILABILITY**
  - Lead contact
  - Materials availability
  - Data and code availability
- **EXPERIMENTAL MODEL AND SUBJECT PARTICIPANT DETAILS**
  - Cell lines and culture
- **METHOD DETAILS**
  - Chemicals
  - Viral production
  - Gene overexpression
  - Gene knockout
  - RNA extraction and quantitative reverse transcription-PCR (qRT-PCR)
  - Protein extraction and western blot analysis
  - Transwell assay
  - Immunostaining
  - RNA sequencing (RNA-seq)
  - Gene set enrichment analysis (GSEA)
  - Stable isotope labeling by amino acids in cell culture (SILAC)
  - LC-MS analysis
  - Immunoprecipitation
  - Chromatin immunoprecipitation (ChIP)
  - Chromatin immunoprecipitation-sequencing (ChIP-seq)
  - Hi-C chromatin immunoprecipitation (Hi-ChIP)
  - Assay for transposase-accessible chromatin (ATAC)
  - Cleavage under targets and release using nuclease (CUT&RUN)
- **QUANTIFICATION AND STATISTICAL ANALYSIS**
  - Data analysis
  - ATAC sequencing (ATAC-seq) analysis
  - ChIP-seq analysis
  - Hi-ChIP analysis
  - CUT&RUN analysis
  - Principal component analysis (PCA)
  - Enrichr analysis
  - Motif analysis

#### SUPPLEMENTAL INFORMATION

Supplemental information can be found online at <https://doi.org/10.1016/j.celrep.2023.113541>.

#### ACKNOWLEDGMENTS

We thank the members of the Sanda laboratory for discussions and critical reviews and Ms. Stella Amanda for illustrations. This research is supported by the National Medical Research Council of the Singapore Ministry of Health (MOH-000525-00: T.S.), the National Research Foundation Singapore, and the Singapore Ministry of Education under its Research Centres of Excellence initiative (T.S.).

#### AUTHOR CONTRIBUTIONS

L.W., H.K., and D.K. performed the experiments; T.K.T. conducted the bioinformatic analyses; S.H.T., A.T.L., and T.S. supervised the study; and L.W. and T.S. wrote the manuscript.

#### DECLARATION OF INTERESTS

All authors declare no conflicts of interest.

Received: May 19, 2023

Revised: October 9, 2023

Accepted: November 20, 2023

Published: December 5, 2023

#### REFERENCES

1. Jansky, S., Sharma, A.K., Korber, V., Quintero, A., Toprak, U.H., Wecht, E.M., Gartlgruber, M., Greco, A., Chomsky, E., Grunewald, T.G.P., et al. (2021). Single-cell transcriptomic analyses provide insights into the developmental origins of neuroblastoma. *Nat. Genet.* **53**, 683–693.
2. Kameneva, P., Artemov, A.V., Kastrioti, M.E., Faure, L., Olsen, T.K., Otte, J., Erickson, A., Semsch, B., Andersson, E.R., Ratz, M., et al. (2021). Single-cell transcriptomics of human embryos identifies multiple sympathoblast lineages with potential implications for neuroblastoma origin. *Nat. Genet.* **53**, 694–706.
3. Boeva, V., Louis-Brennetot, C., Peltier, A., Durand, S., Pierre-Eugene, C., Raynal, V., Etchevers, H.C., Thomas, S., Lermine, A., Daudigeos-Dubus, E., et al. (2017). Heterogeneity of neuroblastoma cell identity defined by transcriptional circuitries. *Nat. Genet.* **49**, 1408–1413.
4. van Groningen, T., Koster, J., Valentijn, L.J., Zwijnenburg, D.A., Akogul, N., Hasselt, N.E., Broekmans, M., Haneveld, F., Nowakowska, N.E., Bras, J., et al. (2017). Neuroblastoma is composed of two super-enhancer-associated differentiation states. *Nat. Genet.* **49**, 1261–1266.
5. van Groningen, T., Akogul, N., Westerhout, E.M., Chan, A., Hasselt, N.E., Zwijnenburg, D.A., Broekmans, M., Stroeken, P., Haneveld, F., Hooijer, G.K.J., et al. (2019). A NOTCH feed-forward loop drives reprogramming from adrenergic to mesenchymal state in neuroblastoma. *Nat. Commun.* **10**, 1530.
6. Shi, H., Tao, T., Abraham, B.J., Durbin, A.D., Zimmerman, M.W., Kadoch, C., and Look, A.T. (2020). ARID1A loss in neuroblastoma promotes the adrenergic-to-mesenchymal transition by regulating enhancer-mediated gene expression. *Sci. Adv.* **6**, eaaz3440.
7. Wang, L., Tan, T.K., Durbin, A.D., Zimmerman, M.W., Abraham, B.J., Tan, S.H., Ngoc, P.C.T., Weichert-Leahey, N., Akahane, K., Lawton, L.N., et al. (2019). ASCL1 is a MYCN- and LMO1-dependent member of the adrenergic neuroblastoma core regulatory circuitry. *Nat. Commun.* **10**, 5622.
8. Guillemot, F., Lo, L.C., Johnson, J.E., Auerbach, A., Anderson, D.J., and Joyner, A.L. (1993). Mammalian achaete-scute homolog 1 is required for the early development of olfactory and autonomic neurons. *Cell* **75**, 463–476.
9. Hanemaaijer, E.S., Margaritis, T., Sanders, K., Bos, F.L., Candelli, T., Al-Saati, H., van Noesel, M.M., Meyer-Wentrup, F.A.G., van de Wetering, M., Holstege, F.C.P., and Clevers, H. (2021). Single-cell atlas of developing murine adrenal gland reveals relation of Schwann cell precursor signature to neuroblastoma phenotype. *Proc. Natl. Acad. Sci. USA* **118**.
10. Dong, R., Yang, R., Zhan, Y., Lai, H.D., Ye, C.J., Yao, X.Y., Luo, W.Q., Cheng, X.M., Miao, J.J., Wang, J.F., et al. (2020). Single-Cell Characterization of Malignant Phenotypes and Developmental Trajectories of Adrenal Neuroblastoma. *Cancer Cell* **38**, 716–733.e6.
11. Vierbuchen, T., Ostermeier, A., Pang, Z.P., Kokubu, Y., Sudhof, T.C., and Wernig, M. (2010). Direct conversion of fibroblasts to functional neurons by defined factors. *Nature* **463**, 1035–1041.
12. Morris, S.A. (2016). Direct lineage reprogramming via pioneer factors; a detour through developmental gene regulatory networks. *Development* **143**, 2696–2705.

13. Park, N.I., Guilhamon, P., Desai, K., McAdam, R.F., Langille, E., O'Connor, M., Lan, X., Whetstone, H., Coutinho, F.J., Vanner, R.J., et al. (2017). ASCL1 Reorganizes Chromatin to Direct Neuronal Fate and Suppress Tumorigenicity of Glioblastoma Stem Cells. *Cell Stem Cell* 21, 209–224.
14. Raposo, A., Vasconcelos, F.F., Drechsel, D., Marie, C., Johnston, C., Dolle, D., Bithell, A., Gillotin, S., van den Berg, D.L.C., Ettwiller, L., et al. (2015). Ascl1 Coordinately Regulates Gene Expression and the Chromatin Landscape during Neurogenesis. *Cell Rep.* 10, 1544–1556.
15. Wapinski, O.L., Lee, Q.Y., Chen, A.C., Li, R., Corces, M.R., Ang, C.E., Treutlein, B., Xiang, C., Baubet, V., Suchy, F.P., et al. (2017). Rapid Chromatin Switch in the Direct Reprogramming of Fibroblasts to Neurons. *Cell Rep.* 20, 3236–3247.
16. Wapinski, O.L., Vierbuchen, T., Qu, K., Lee, Q.Y., Chanda, S., Fuentes, D.R., Giresi, P.G., Ng, Y.H., Marro, S., Neff, N.F., et al. (2013). Hierarchical mechanisms for direct reprogramming of fibroblasts to neurons. *Cell* 155, 621–635.
17. Zimmerman, M.W., Liu, Y., He, S., Durbin, A.D., Abraham, B.J., Easton, J., Shao, Y., Xu, B., Zhu, S., Zhang, X., et al. (2018). MYC Drives a Subset of High-Risk Pediatric Neuroblastomas and Is Activated through Mechanisms Including Enhancer Hijacking and Focal Enhancer Amplification. *Cancer Discov.* 8, 320–335.
18. Meyers, E.A., and Kessler, J.A. (2017). TGF- $\beta$  Family Signaling in Neural and Neuronal Differentiation, Development, and Function. *Cold Spring Harbor Perspect. Biol.* 9.
19. Muroyama, Y., Fujihara, M., Ikeya, M., Kondoh, H., and Takada, S. (2002). Wnt signaling plays an essential role in neuronal specification of the dorsal spinal cord. *Genes Dev.* 16, 548–553.
20. Lee, Q.Y., Mall, M., Chanda, S., Zhou, B., Sharma, K.S., Schaukowitz, K., Adrian-Segarra, J.M., Grieder, S.D., Karetka, M.S., Wapinski, O.L., et al. (2020). Pro-neuronal activity of Myod1 due to promiscuous binding to neuronal genes. *Nat. Cell Biol.* 22, 401–411.
21. Persson, P., Jogi, A., Grynfeld, A., Pahlman, S., and Axelson, H. (2000). HASH-1 and E2-2 are expressed in human neuroblastoma cells and form a functional complex. *Biochem. Biophys. Res. Commun.* 274, 22–31.
22. Ellenberger, T., Fass, D., Arnaud, M., and Harrison, S.C. (1994). Crystal structure of transcription factor E47: E-box recognition by a basic region helix-loop-helix dimer. *Genes Dev.* 8, 970–980.
23. Hayashi, Y., Hsiao, E.C., Sami, S., Lancero, M., Schlieve, C.R., Nguyen, T., Yano, K., Nagahashi, A., Ikeya, M., Matsumoto, Y., et al. (2016). BMP-SMAD-ID promotes reprogramming to pluripotency by inhibiting p16/INK4A-dependent senescence. *Proc. Natl. Acad. Sci. USA* 113, 13057–13062.
24. Nakashima, K., Takizawa, T., Ochiai, W., Yanagisawa, M., Hisatsune, T., Nakafuku, M., Miyazono, K., Kishimoto, T., Kageyama, R., and Taga, T. (2001). BMP2-mediated alteration in the developmental pathway of fetal mouse brain cells from neurogenesis to astrocytogenesis. *Proc. Natl. Acad. Sci. USA* 98, 5868–5873.
25. Hollnagel, A., Oehlmann, V., Heymer, J., Ruther, U., and Nordheim, A. (1999). Id genes are direct targets of bone morphogenetic protein induction in embryonic stem cells. *J. Biol. Chem.* 274, 19838–19845.
26. Ellis, H.M., Spann, D.R., and Posakony, J.W. (1990). extramacrochaetae, a negative regulator of sensory organ development in *Drosophila*, defines a new class of helix-loop-helix proteins. *Cell* 61, 27–38.
27. Garrell, J., and Modolell, J. (1990). The *Drosophila* extramacrochaetae locus, an antagonist of proneural genes that, like these genes, encodes a helix-loop-helix protein. *Cell* 61, 39–48.
28. Gartlgruber, M., Sharma, A.K., Quintero, A., Dreidax, D., Jansky, S., Park, Y.G., Kreth, S., Meder, J., Doncevic, D., Saary, P., et al. (2021). Super enhancers define regulatory subtypes and cell identity in neuroblastoma. *Nat. Can. (Ott.)* 2, 114–128.
29. Parkinson, L.M., Gillen, S.L., Woods, L.M., Chaytor, L., Marcos, D., Ali, F.R., Carroll, J.S., and Philpott, A. (2022). The proneural transcription factor ASCL1 regulates cell proliferation and primes for differentiation in neuroblastoma. *Front. Cell Dev. Biol.* 10, 942579.
30. Woods, L.M., Ali, F.R., Gomez, R., Chernukhin, I., Marcos, D., Parkinson, L.M., Tayoun, A.N.A., Carroll, J.S., and Philpott, A. (2022). Elevated ASCL1 activity creates de novo regulatory elements associated with neuronal differentiation. *BMC Genomics* 23, 255.
31. Oldridge, D.A., Wood, A.C., Weichert-Leahey, N., Crimmins, I., Sussman, R., Winter, C., McDaniel, L.D., Diamond, M., Hart, L.S., Zhu, S., et al. (2015). Genetic predisposition to neuroblastoma mediated by a LMO1 super-enhancer polymorphism. *Nature* 528, 418–421.
32. Wang, K., Diskin, S.J., Zhang, H., Attiyeh, E.F., Winter, C., Hou, C., Schnepf, R.W., Diamond, M., Bosse, K., Mayes, P.A., et al. (2011). Integrative genomics identifies LMO1 as a neuroblastoma oncogene. *Nature* 469, 216–220.
33. Schwab, M., Alitalo, K., Klempnauer, K.H., Varmus, H.E., Bishop, J.M., Gilbert, F., Brodeur, G., Goldstein, M., and Trent, J. (1983). Amplified DNA with limited homology to myc cellular oncogene is shared by human neuroblastoma cell lines and a neuroblastoma tumour. *Nature* 305, 245–248.
34. Kohl, N.E., Kanda, N., Schreck, R.R., Bruns, G., Latt, S.A., Gilbert, F., and Alt, F.W. (1983). Transposition and amplification of oncogene-related sequences in human neuroblastomas. *Cell* 35, 359–367.
35. Aubrey, B.J., Kelly, G.L., Kueh, A.J., Brennan, M.S., O'Connor, L., Milla, L., Wilcox, S., Tai, L., Strasser, A., and Herold, M.J. (2015). An inducible lentiviral guide RNA platform enables the identification of tumor-essential genes and tumor-promoting mutations in vivo. *Cell Rep.* 10, 1422–1432.
36. Schneider, C.A., Rasband, W.S., and Eliceiri, K.W. (2012). NIH Image to ImageJ: 25 years of image analysis. *Nat. Methods* 9, 671–675.
37. Langmead, B., and Salzberg, S.L. (2012). Fast gapped-read alignment with Bowtie 2. *Nat. Methods* 9, 357–359.
38. Deutsch, E.W., Bandeira, N., Sharma, V., Perez-Riverol, Y., Carver, J.J., Kundu, D.J., Garcia-Seisdedos, D., Jarnuczak, A.F., Hewapathirana, S., Pullman, B.S., et al. (2020). The ProteomeXchange consortium in 2020: enabling 'big data' approaches in proteomics. *Nucleic Acids Res.* 48, D1145–D1152.
39. Perez-Riverol, Y., Xu, Q.W., Wang, R., Uszkoreit, J., Griss, J., Sanchez, A., Reisinger, F., Csordas, A., Tement, T., Del-Toro, N., et al. (2016). PRIDE Inspector Toolsuite: Moving Toward a Universal Visualization Tool for Proteomics Data Standard Formats and Quality Assessment of ProteomeXchange Datasets. *Mol. Cell. Proteomics* 15, 305–317.
40. Perez-Riverol, Y., Bai, J., Bandla, C., Garcia-Seisdedos, D., Hewapathirana, S., Kamachinathan, S., Kundu, D.J., Prakash, A., Frericks-Zipper, A., Eisenacher, M., et al. (2022). The PRIDE database resources in 2022: a hub for mass spectrometry-based proteomics evidences. *Nucleic Acids Res.* 50, D543–D552.
41. Mootha, V.K., Lindgren, C.M., Eriksson, K.F., Subramanian, A., Sihag, S., Lehar, J., Puigserver, P., Carlsson, E., Ridderstrale, M., Laurila, E., et al. (2003). PGC-1 $\alpha$ -responsive genes involved in oxidative phosphorylation are coordinately downregulated in human diabetes. *Nat. Genet.* 34, 267–273.
42. Subramanian, A., Tamayo, P., Mootha, V.K., Mukherjee, S., Ebert, B.L., Gillette, M.A., Paulovich, A., Pomeroy, S.L., Golub, T.R., Lander, E.S., and Mesirov, J.P. (2005). Gene set enrichment analysis: a knowledge-based approach for interpreting genome-wide expression profiles. *Proc. Natl. Acad. Sci. USA* 102, 15545–15550.
43. Cox, J., and Mann, M. (2008). MaxQuant enables high peptide identification rates, individualized p.p.b.-range mass accuracies and proteome-wide protein quantification. *Nat. Biotechnol.* 26, 1367–1372.

44. Pimentel, H., Bray, N.L., Puente, S., Melsted, P., and Pachter, L. (2017). Differential analysis of RNA-seq incorporating quantification uncertainty. *Nat. Methods* *14*, 687. <https://www.nature.com/articles/nmeth.4324#supplementary-information>.
45. Babicki, S., Arndt, D., Marcu, A., Liang, Y., Grant, J.R., Maciejewski, A., and Wishart, D.S. (2016). Heatmapper: web-enabled heat mapping for all. *Nucleic Acids Res.* *44*, W147–W153.
46. Ramirez, F., Ryan, D.P., Gruning, B., Bhardwaj, V., Kilpert, F., Richter, A.S., Heyne, S., Dundar, F., and Manke, T. (2016). deepTools2: a next generation web server for deep-sequencing data analysis. *Nucleic Acids Res.* *44*, W160–W165.
47. Zhu, Q., Liu, N., Orkin, S.H., and Yuan, G.C. (2019). CUT&RUNTools: a flexible pipeline for CUT&RUN processing and footprint analysis. *Genome Biol.* *20*, 192.

STAR★METHODS

KEY RESOURCES TABLE

REAGENT or RESOURCE	SOURCE	IDENTIFIER
<b>Antibodies</b>		
Anti-ASCL1, mouse monoclonal	Santa Cruz	Cat# sc-374104; RRID: AB_10918561
Anti-DLL3, rabbit monoclonal	Cell Signaling Technologies	Cat# 71804; RRID: AB_2799809
Anti-FN1, mouse monoclonal	Santa Cruz	Cat# sc-69681; RRID: AB_1122900
Anti-FRA1, mouse monoclonal	Santa Cruz	Cat# sc-28310; RRID: AB_627632
Anti-H3, mouse monoclonal	Cell Signaling Technologies	Cat# 3638; RRID: AB_1642229
Anti-H3K27ac, rabbit polyclonal	abcam	Cat# ab4729; RRID: AB_2118291
Anti-HA, rabbit monoclonal	Cell Signaling Technologies	Cat# 3724; RRID: AB_1549585
Anti-HEB, rabbit polyclonal	Santa Cruz	Cat# sc-357; RRID: AB_671268
Anti-ID3, rabbit polyclonal	Santa Cruz	Cat# sc-490; RRID: AB_2123010
Anti-ISL1, mouse monoclonal	Santa Cruz	Cat# sc-390793; RRID: AB_2916082
Anti-LMO1, rabbit polyclonal	Bethyl Laboratories	Cat# A300314A; RRID: AB_309463
Anti-Mouse IgG, mouse	Santa Cruz	Cat# sc-2025; RRID: AB_737182
Anti-Mouse IgG HRP-conjugated, horse polyclonal	Cell Signaling Technologies	Cat# 7076; RRID: AB_330924
Anti-MYC, rabbit monoclonal	Cell Signaling Technologies	Cat# 5605; RRID: AB_1903938
Anti-MYCN, rabbit monoclonal	Cell Signaling Technologies	Cat# 84406; RRID: AB_2800038
Anti-PHOX2B, mouse monoclonal	Santa Cruz	Cat# sc-376997; RRID: AB_2813765
Anti-Rabbit IgG, rabbit	Cell Signaling Technologies	Cat# 2729; RRID: AB_1031062
Anti-Rabbit IgG HRP-conjugated, goat polyclonal	Cell Signaling Technologies	Cat# 7074; RRID: AB_2099233
Anti-SMAD1, rabbit monoclonal	Cell Signaling Technologies	Cat# 6944; RRID: AB_10858882
Anti-SMAD1/5 (phospho-Ser463/465), rabbit monoclonal	Cell Signaling Technologies	Cat# 9516; RRID: AB_491015
Anti-SMAD2 (phospho-Ser465/467), rabbit monoclonal	Cell Signaling Technologies	Cat# 3108; RRID: AB_490941
Anti-SMAD2/3, rabbit monoclonal	Cell Signaling Technologies	Cat# 8685; RRID: AB_10889933
Anti-SMAD3 (phospho-Ser423/425), rabbit monoclonal	Cell Signaling Technologies	Cat# 9520; RRID: AB_2193207
Anti-TCF3, mouse monoclonal	BD Pharmingen	Cat# 554199; RRID: AB_395298
Anti-TCF4, rabbit polyclonal	Proteintech	Cat# 22337-1-AP; RRID: AB_2879076
Anti-( $\alpha$ -Tubulin, mouse monoclonal	Cell Signaling Technologies	Cat# 3873; RRID: AB_1904178
Anti-( $\alpha$ -Actin, mouse monoclonal	Cell Signaling Technologies	Cat# 3700; RRID: AB_2242334
Anti-( $\alpha$ -Catenin, rabbit monoclonal	Cell Signaling Technologies	Cat# 8480; RRID: AB_11127855
Anti-( $\alpha$ -Catenin (phospho-Ser675), rabbit monoclonal	Cell Signaling Technologies	Cat# 4176; RRID: AB_1903923
<b>Bacterial and virus strains</b>		
DH5-a chemically competent <i>Escherichia coli</i>	Invitrogen, Thermo Fisher Scientific	Cat# 18265017
One Shot Stbl3, chemically competent <i>Escherichia coli</i>	Invitrogen, Thermo Fisher Scientific	Cat# C737303
One Shot Mach1-T1R chemically competent <i>Escherichia coli</i>	Invitrogen, Thermo Fisher Scientific	Cat# K243520
One Shot ccdB Survival 2 T1R Competent Cells	Invitrogen, Thermo Fisher Scientific	Cat# A10460

(Continued on next page)

**Continued**

REAGENT or RESOURCE	SOURCE	IDENTIFIER
<b>Chemicals, peptides, and recombinant proteins</b>		
RepSox, TGF $\beta$ R-1/ALK5 inhibitor	MedChem Express	Cat# HY-13012
LDN193189, BMP type I receptor inhibitor	MedChem Express	Cat# HY-12071
Dimethyl sulfoxide (DMSO)	Sigma-Aldrich	Cat# D2650
Doxycycline hydrochloride	Sigma-Aldrich	Cat# D3072
HEPES	Gibco	Cat# L0180-100
Roswell Park Memorial Institute (RPMI) 1640 medium w/L-glutamine	Biowest	Cat# L0500-500
Dulbecco's Modified Eagle's medium (DMEM) high glucose w/L-glutamine w/sodium pyruvate	Biowest	Cat# L0104-500
Penicillin/Streptomycin	Biowest	Cat# L0022-100
Trypsin-EDTA 10X	Biowest	Cat# X0930-100
Polybrene infection/transfection Reagent	Sigma-Aldrich	Cat# TR-1003-G
Hygromycin B, from <i>Streptomyces hygroscopicus</i>	Sigma-Aldrich	Cat# H7772-1g
Puromycin dihydrochloride	Sigma-Aldrich	Cat# P9620
Blasticidin S HCl	Thermo Fisher Scientific	Cat# A1113903
Geneticin Selective Antibiotic (G418 Sulfate)	Thermo Fisher Scientific	Cat# 10131035
Bromodeoxyuridine (BrdU)	Biologend	Cat# 423401
Propidium iodide solution	Sigma-Aldrich	Cat# P4864
AMPure XP Reagent	Beckman Coulter	Cat# A63880
Dynabeads Protein A	Invitrogen, Thermo Fisher Scientific	Cat#10002D
Dynabeads Protein G	Invitrogen, Thermo Fisher Scientific	Cat#10003D
Fetal Bovine Serum (South America), Tetracycline Free	Biowest	Cat# S181T-500
Fetal Bovine Serum (South America)	Biowest	Cat# S1810-500
PowerUp™ SYBR™ Green Master Mix	Thermo Fisher Scientific	Cat# A25778
QIAzol Lysis Reagent	QIAGEN	Cat# 79306
Cell Lysis Buffer (10X)	Cell Signaling Technologies	Cat# 9806
CutSmart restriction digestion buffer	New England Biolabs	Cat# B7204
IGEPAL CA-630	Merck, Sigma-Aldrich	Cat# I8896
Formaldehyde solution (37%)	Sigma-Aldrich	Cat# F8775
Fugene6 Transfection Reagent	Promega	Cat# E2691
ECL™ Select Western Blotting Detection Reagent	Cytiva	Cat# RPN2235
Halt™ Protease Inhibitor Cocktail, EDTA-Free (100X)	Thermo Fisher Scientific	Cat# 78439
T4 DNA Ligase	New England Biolabs	Cat# M0202L
<b>Critical commercial assays</b>		
CellTiter-Glo Luminescent Cell Viability Assay	Promega	Cat# G7572
Arima Hi-ChIP Kit	Arima Genomics	N/A
miRNeasy Kits	QIAGEN	Cat# 217004
RNeasy MinElute Cleanup Kit	QIAGEN	Cat# 74204

(Continued on next page)

<b>Continued</b>		
REAGENT or RESOURCE	SOURCE	IDENTIFIER
GeneJET Plasmid Miniprep Kit	Thermo Fisher Scientific	Cat# K0502
Zymogen ChIP DNA Clean and Concentrator Kit	Zymo Research	Cat# D5205
NucleoSpin RNA Mini Kit for RNA Purification	Macherey-Nagel	Cat# 740955.250
Illumina Tagment DNA Enzyme and Buffer Small Kit	Illumina	Cat# 20034197
CUTANA ChIC/CUT&RUN Kit	EpiCypher	Cat# 14-1048
NEBNext Multiplex Oligos for Illumina (Index Primers)	New England Biolabs	Cat# E7335
NEBNext Ultra II DNA Library Prep Kit	New England Biolabs	Cat# E7645
<b>Deposited data</b>		
RNA-seq	This paper	GEO: GSE214796
ChIP-seq	This paper	GEO: GSE214796
Proteomic	This paper	PRIDE: PXD037670
ATAC-seq	This paper	GEO: GSE214796
Hi-ChIP	This paper	GEO: GSE214796
<b>Experimental models: Cell lines</b>		
Human: GI-MEN	DSMZ	Cat# ACC 654
Human: SH-EP	Laboratory of Thomas Look	N/A
Human: HEK293T	ATCC	Cat# CRL-11268; RRID: CVCL_0063
Human: Kelly	Laboratory of Thomas Look	N/A
Human: CHP-134	DSMZ	Cat# ACC 653
Human: SK-N-DZ	ATCC	Cat# CRL-2149
Human: SK-N-SH	Laboratory of Thomas Look	N/A
<b>Oligonucleotides</b>		
Scrambled sgRNA (sgSCR) for Human cells	This paper	N/A
sgRNA-1 targeting Human TCF12	This paper	N/A
sgRNA-1 targeting Human TCF3	This paper	N/A
<b>Recombinant DNA</b>		
MSCV-PHOX2B-Blasticidin expression vector	This paper	N/A
MSCV-MYCN-GFP expression vector	This paper	N/A
MSCV-ISL1-Hygromycin expression vector	This paper	N/A
MSCV-LMO1-Neomycin expression vector	This paper	N/A
pCW57.1-Puro expression vector	Laboratory of David Root	Addgene Cat#41393
FgH1tUTG-GFP sgRNA expression vector	Aubrey et al., 2015 <sup>35</sup>	Addgene Cat#70183
<b>Software and algorithms</b>		
ImageJ	Schneider et al., 2012 <sup>36</sup>	<a href="https://imagej.nih.gov/ij/">https://imagej.nih.gov/ij/</a>
Bowtie2	Langmead and Salzberg, 2012 <sup>37</sup>	<a href="http://bowtie-bio.sourceforge.net/bowtie2/index.shtml">http://bowtie-bio.sourceforge.net/bowtie2/index.shtml</a>

## RESOURCE AVAILABILITY

### Lead contact

Further information and requests for resources and reagents should be directed to and will be fulfilled by the lead contact, Takaomi Sanda ([takaomi\\_sanda@u.nus.edu](mailto:takaomi_sanda@u.nus.edu)).

### Materials availability

All custom plasmids generated from this study will be available upon request.

### Data and code availability

All relevant data are available from the authors. All software used in this work is described in the relevant STAR Methods sections. The RNA-seq, ChIP-seq, CUT&RUN, ATAC-seq and Hi-ChIP data have been deposited (GEO: GSE214796). The datasets used for ASCL1 and H3K27ac ChIP-seq in Kelly cells were from our previous publication and were obtained from the GEO database (GSE120074 and GSE62726). The mass spectrometry proteomics data have been deposited to the ProteomeXchange Consortium<sup>38,39</sup> via the PRIDE<sup>40</sup> partner repository with the dataset identifier PXD037670.

## EXPERIMENTAL MODEL AND SUBJECT PARTICIPANT DETAILS

### Cell lines and culture

All cell lines were confirmed by DNA fingerprinting using the PowerPlex 1.2 system (Promega, Madison, WI, USA) and were regularly tested for mycoplasma contamination.

All neuroblastoma cell lines (GI-MEN, SH-EP, Kelly, SK-N-DZ, CHP-134 and SK-N-SH) were cultured in RPMI 1640 medium (Biowest, cat# L0500-500) supplemented with 10% fetal bovine serum (FBS; Biowest, cat# S1810-500) and 1% penicillin/streptomycin (Biowest, cat# L0022-020). GI-MEN cell lines transduced with the DOX-inducible pCW57.1-ASCL1 vector were cultured in RPMI 1640 medium (Biowest, cat# L0500-500) supplemented with 10% tetracycline-free fetal bovine serum (Biowest, cat# S181T-500) and 1% penicillin/streptomycin (Biowest, cat# L0022-020). HEK293T cells were cultured in DMEM (Biowest, cat# L0104-500) supplemented with 10% fetal bovine serum (Biowest, cat# S1810-500) and 1% penicillin/streptomycin (Biowest, cat# L0022-020). All cell lines were grown at 37°C with 5% CO<sub>2</sub>.

## METHOD DETAILS

### Chemicals

Doxycycline hydrochloride was purchased from Sigma-Aldrich and dissolved in DMSO. LDN-193189 and RepSox were purchased from MedChemExpress and dissolved in DMSO.

### Viral production

Retrovirus was produced in HEK293T cells. HEK293T cells ( $0.2 \times 10^6$ ) were plated in a single well of a 6-well plate 24 h prior to transfection. The retroviral vector (1,000 ng) was cotransfected with the packaging plasmid pMD-MLV (250 ng) and the envelope plasmid VSV-G (250 ng) into HEK293T cells using FuGene 6 transfection reagent (Promega, cat# E2691) and Opti-MEM (Gibco, cat# 31985062) according to the manufacturer's instructions. The medium was changed 24 h after transfection.

Similarly, lentivirus was produced in HEK293T cells. HEK293T cells ( $0.2 \times 10^6$ ) were plated in a single well of a 6-well plate 24 h prior to transfection. The lentiviral vector (500 ng) was co-transfected with the packaging plasmids pMDLg/pRRE (250 ng) and pRSV-Rev (250 ng) and the envelope plasmid pMD2.G (250 ng) using FuGene 6 transfection reagent (Promega, cat# E2691) and Opti-MEM (Gibco, cat# 31985062) according to the manufacturer's instructions. The medium was replaced 24 h after transfection.

Supernatants containing retrovirus or lentivirus were collected 48 and 72 h posttransfection, combined, filtered through a 0.45 mm nitrocellulose filter (Thermo), and stored at  $-80^\circ\text{C}$ .

### Gene overexpression

ASCL1 cDNA (CDS region of the ASCL1 transcript, NM\_004316.4) was amplified and cloned into the Tet-on pCW57.1 lentiviral vector. LMO1, ISL1, PHOX2B and MYCN cDNA (CDS region of the LMO1 transcript, NM\_001270428.1; CDS region of the ISL1 transcript, NM\_002202.3; CDS region of the PHOX2B transcript, NM\_003924.4; CDS region of the MYCN transcript, NM\_001293228.2) were amplified and cloned into the retroviral vectors pMSCV-IRES-Neomycin, pMSCV-IRES-Hygromycin, pMSCV-IRES-Blasticidin, and pMSCV-IRES-GFP, respectively. Approximately 500,000 cells were transduced with 1 mL of virus-containing medium in the presence of 8  $\mu\text{g}$  of polybrene (8  $\mu\text{g}/\text{mL}$ ; Millipore) and 10  $\mu\text{L}$  of 1 M HEPES (10  $\mu\text{L}/\text{mL}$ , Gibco) by incubation for 2 h followed by topping up with 1 mL of fresh medium. The cells that expressed GFP were then sorted by flow cytometry using a BD FACSAria II cell sorter (BD Biosciences). The cells expressing drug selection markers were then selected with puromycin (1  $\mu\text{g}/\text{mL}$ ), neomycin (300  $\mu\text{g}/\text{mL}$ ), hygromycin (25  $\mu\text{g}/\text{mL}$ ) or blasticidin (5  $\mu\text{g}/\text{mL}$ ).

### Gene knockout

The CRISPR/Cas9 system was used to knock out the TCF12 and TCF3 genes. To express the Cas9 protein, lentivirus was produced using the FUCas9Cherry lentiviral vector. GI-MEN cells were infected with virus-containing medium using the method mentioned in the previous section. The cells that expressed mCherry were then sorted by flow cytometry using the BD FACSAria II (BD Biosciences). Subsequently, Cas9-expressing cells were transduced with an inducible sgRNA and the GFP gene sequence. The sgRNA sequences were designed using the CRISPR Design Tool (<http://crispr.mit.edu/>) and cloned into the FgH1tUTG lentiviral vector (Addgene #70183) at the BmsBI restriction site. The cells expressing GFP were selected by evaluation for the GFP signal by flow cytometry using the BD FACSAria II (BD Biosciences). The cells were then treated with 1,000 ng/mL DOX to induce sgRNA expression. The sgRNA sequences are shown in Table S7.

### RNA extraction and quantitative reverse transcription-PCR (qRT-PCR)

Total RNA was extracted using a NucleoSpin RNA Kit (Macherey-Nagel). A total of 1,000 ng of purified RNA was reverse transcribed into cDNA in a 10  $\mu$ L reaction volume and finally diluted to 50  $\mu$ L using an EvoScript Universal cDNA Master Kit (Roche) according to the manufacturer's guidelines. The total 20  $\mu$ L volume of PCR mix contained 2  $\mu$ L of cDNA, 10  $\mu$ L of Power SYBR Green PCR Master Mix (Roche), and 1  $\mu$ L each of the forward primer and reverse primer (final concentration of 500 nM). The mRNA expression levels of the genes of interest were evaluated by the  $\Delta\Delta$  Ct method after qPCR analysis with a Quant Studio 3 Real-Time PCR System (Thermo Fisher Scientific) with the following thermal cycling conditions: 2 min at 50°C, 10 min at 95°C, and 1 min at 60°C, with a temperature ramp of 1.6°C/s. Primers were tested by construction of a standard curve with serially diluted DNA to ensure an efficiency of between 90% and 110%, an  $R^2$  for the standard curve of greater than 0.95 and a single peak on the melt curve to ensure primer specificity. The primer sequences for amplification of each gene are shown in [Table S7](#).

### Protein extraction and western blot analysis

Cells were lysed using Cell Lysis Buffer (20 mM Tris-HCl (pH 7.5), 150 mM NaCl, 1 mM Na<sub>2</sub>EDTA, 1 mM EGTA, 1% NP-40, 1% sodium deoxycholate, 2.5 mM sodium pyrophosphate, 1 mM beta-glycerophosphate, 1 mM Na<sub>3</sub>VO<sub>4</sub>, and 1  $\mu$ g/mL leupeptin) (#9803, Cell Signaling Technologies) with protease inhibitors (Roche). The protein concentration was measured using Bio-Rad reagent (Life Technologies). Protein lysate (20  $\mu$ g) was diluted in Laemmli sample buffer (Bio-Rad) with 10%  $\beta$ -mercaptoethanol and boiled for 10 min at 95°C. Proteins were resolved by SDS-PAGE in running buffer (Bio-Rad) using a Bio-Rad system and subsequently transferred onto PVDF membranes (Bio-Rad). Membranes were blocked with 5% nonfat milk for 1 h and washed with washing buffer (TBS-Tween 0.1%) following incubation with a primary antibody diluted in 5% BSA (P6154, Biowest) dissolved in washing buffer overnight at 4°C. Incubation with secondary antibodies was performed after washing for 1 h at room temperature. HRP-conjugated anti-rabbit (7074, Cell Signaling Technologies; 1:10,000 dilution) and anti-mouse (7076P2, Cell Signaling; 1:10,000 dilution) antibodies were used. The membranes were finally incubated with ECL solution (RPN2236, Amersham ECL Prime Western Blotting Detection Reagent) and imaged with a Bio-Rad ChemiDoc imaging system. Antibodies specific for the following proteins were used for immunoblotting: FN1 (Santa Cruz, 1:200 dilution, sc-69681), FRA1 (Santa Cruz, 1:200 dilution, sc-376148), DLL3 (Cell Signaling Technologies, 1:1000 dilution, #2483), TCF12 (Santa Cruz, 1:200 dilution, #sc-365980), TCF3 (BD Biosciences, 1:1000 dilution, #554077), TCF4 (Proteintech, 1:1000 dilution, 22337-1-AP), MYC (Cell Signaling Technologies, 1:1000 dilution, #5605), ID3 (Santa Cruz, 1:200 dilution, sc-490), phospho-SMAD2/3 (Cell Signaling Technologies, 1:1000 dilution, #8828), SMAD2/3 (Cell Signaling Technologies, 1:1000 dilution, #8685), phospho-SMAD1 (Cell Signaling Technologies, 1:1000 dilution, #9516), SMAD1 (Cell Signaling Technologies, 1:1000 dilution, #9743),  $\beta$ -catenin (Cell Signaling Technologies, 1:1000 dilution, #8480), phospho- $\beta$ -catenin (Cell Signaling Technologies, 1:1000 dilution, #9566), PHOX2B (Santa Cruz, 1:200 dilution, #sc-376997), ISL1 (Santa Cruz, 1:200 dilution, #sc-390793), LMO1 (Bethyl Laboratories, 1:1000 dilution, #A300314A), ASCL1 (Santa Cruz, 1:200 dilution, #sc-390794), MYCN (Cell Signaling Technologies, 1:1000 dilution, #84406),  $\alpha$ -tubulin (Cell Signaling Technologies, 1:1000 dilution, #2144) and  $\beta$ -actin (Cell Signaling Technologies, 1:1000 dilution, #8457).

### Transwell assay

The Transwell assay was carried out with 8.0- $\mu$ m pore size Transwell inserts (Corning, #3403). A total of 10,000 GI-MEN cells were seeded into the upper compartment of each Transwell insert in serum-free RPMI 1640 medium. RPMI 1640 medium supplemented with 10% FBS was added to the lower compartments. Cells were incubated in the Transwell chambers for 48 h and subjected to staining with 0.1% crystal violet. The cells on the upper surface of each membrane were gently removed by wiping with a cotton swab. Images of migrated cells in representative fields of view on each membrane were acquired.

### Immunostaining

Cells were washed with warm PBS twice and fixed with 4% formaldehyde solution for 10 min at room temperature. The cells were then washed with PBS twice and permeabilized with 0.2% Triton X- for 10 min at room temperature. The cells were then washed with PBS twice and incubated with 5% donkey serum in PBS buffer at room temperature for 1 h. The cells were then washed again with PBS. The regions for immunostaining were circled with a hydrophobic pen and incubated with a primary antibody overnight at 4°C. The cells were washed with PBS and then incubated with a secondary antibody for 2 h at room temperature. The cells were counterstained with Hoechst dye (33258, Invitrogen) at a final concentration of 0.01 mg/mL. The cells were washed before imaging. Antibodies were diluted with 5% BSA in PBS buffer. An anti-ASCL1 antibody and (Santa Cruz, 1:200 dilution, #sc-390794), donkey anti-rabbit IgG (H + L), Alexa Fluor 488 (A21204, Thermo, 1:1000) were used.

### RNA sequencing (RNA-seq)

Total RNA was extracted from cells using QIAzol Lysis Reagent (QIAGEN) and cleaned using an RNeasy Kit (QIAGEN). Samples were treated with TURBO DNase (TURBO DNA-free Kit; Ambion) and cleaned using an RNeasy MinElute Cleanup Kit (QIAGEN). Strand-specific library construction and Illumina HiSeq sequencing of  $\sim$ 100 M paired-end 100-bp reads were performed at BGI Biotech Solutions Co., Ltd. (Hong Kong, China).

### Gene set enrichment analysis (GSEA)

GSEA<sup>41,42</sup> was performed with the normalized gene expression data with the log<sub>2</sub> ratio of class means metric for comparison between samples of control and ASCL1-overexpressing GI-MEN cells. The direct target genes regulated by ASCL1 in GI-MEN cells were identified by RNA-seq based on a significant change in gene expression (absolute log<sub>2</sub>FC ≥ or ≤ 0.5; adjusted p value < 0.05) upon ASCL1 overexpression.

### Stable isotope labeling by amino acids in cell culture (SILAC)

GI-MEN cells transduced with the inducible ASCL1 construct were cultured in light SILAC medium or heavy SILAC medium separately for at least 14 passages. Heavy SILAC medium was composed of 500 mL of RPMI 1640 medium without Arg and Lys, 5 mL penicillin/streptomycin (100x), 50 mL of dialyzed fetal bovine serum, 500 μL of L-arginine-10 (84 mg/mL) and 170 μL of L-lysine-8 (146 mg/mL). Light SILAC medium was composed of 500 mL of RPMI 1640 medium without Arg and Lys, 5 mL of penicillin/streptomycin (100x), 50 mL of dialyzed fetal bovine serum, 500 μL of L-arginine-0 (84 mg/mL) and 170 μL of L-lysine-0 (146 mg/mL). The prepared media were filtered prior to use. The amino acid incorporation efficiency in the SILAC media was determined to be greater than 98% before the immunoprecipitation step. As described, anti-ASCL1 antibodies and control IgG were used for the immunoprecipitation step. Equal amounts of cells cultured in light SILAC medium and heavy SILAC medium were subjected to immunoprecipitation. Anti-ASCL1 antibody-conjugated beads incubated with lysate from cells cultured in heavy SILAC medium were mixed with IgG-conjugated beads incubated with lysate from cells cultured in light SILAC medium, and vice versa, prior to elution with Laemmli sample buffer (Bio-Rad) containing 10% β-mercaptoethanol and boiled for 10 min at 95°C. Samples were then prepared for separation by SDS-PAGE and LC-MS analysis.

### LC-MS analysis

ASCL1 IP samples were separated on a 12% NuPAGE Bis-Tris precast gel (Thermo Fisher Scientific) for 10 min at 170 V in 1x MOPS buffer (Thermo Fisher Scientific). The gel was fixed using the Colloidal Blue Staining Kit (Thermo Fisher Scientific) and each lane was processed as a single sample. For in-gel digestion, samples were destained (25 mM ammonium bicarbonate; 50% ethanol), reduced in 10 mM DTT for 1 h at 56°C followed by alkylation with 55 mM iodoacetamide (Sigma) for 45 min in the dark. Tryptic digestion was performed with 2 μg trypsin (Promega) in 50 mM ammonium bicarbonate buffer at 37°C overnight. Peptides were desalted on StageTips and analyzed by nanoflow liquid chromatography on an EASY-nLC 1200 system coupled to a Q Exactive HF mass spectrometer (Thermo Fisher Scientific). Peptides were separated on a C18-reversed phase column (25 cm long, 75 μm inner diameter) packed in-house with ReproSil-Pur C18-AQ 1.9 μm resin (Dr Maisch). The column was mounted on an Easy Flex Nano Source and temperature controlled by a column oven (Sonation) at 40°C. A 105-min gradient from 2 to 40% acetonitrile in 0.1% formic acid at a flow of 225 nL/min was used. Spray voltage was set to 2.2 kV. The Q Exactive HF was operated with a TOP20 MS/MS spectra acquisition method per MS full scan. MS scans were conducted with 60,000 at a maximum injection time of 20 ms and MS/MS scans with 15,000 resolution at a maximum injection time of 75 ms.

The raw files were processed with MaxQuant version 1.5.2.8 and searched against the human Uniprot database (95,934 entries).<sup>43</sup> Carbamidomethylation was set as fixed modification while methionine oxidation and protein N-acetylation were considered as variable modifications. The re-quantify option was activated. For enzyme specificity, trypsin was selected with a maximum of two mis-cleavages. Search results were filtered with a false discovery rate of 0.01. Known contaminants, proteins groups only identified by site, and reverse hits were removed and only proteins were kept that were quantified by SILAC ratios in both labeling combinations (ASCL1 IP heavy vs. IgG light and ASCL1 light vs. IgG heavy).

### Immunoprecipitation

Approximately 10 million cells were lysed in Cell Lysis Buffer (50 mM Tris (pH 7.5), 150 mM NaCl, 1 mM EDTA, 0.5% NP40, 0.1% SDS 10% glycerol and protease inhibitor cocktail (Roche)). Magnetic beads were precleared with 0.5% BSA in PBS buffer and preincubated with 1 μg of antibodies overnight. The antibody-conjugated beads were washed in PBS buffer and incubated with cell lysate overnight. A portion of the cell lysate was saved as input. The beads were washed with washing buffer. Proteins pulled down by the beads were eluted with Laemmli sample buffer (Bio-Rad) containing 10% β-mercaptoethanol and boiled for 10 min at 95°C. The input sample was mixed with an equal amount of Laemmli sample buffer (Bio-Rad) containing 10% β-mercaptoethanol and boiled for 10 min at 95°C. The protein samples were subjected to Western blot analysis. The antibodies used for immunoprecipitation were as follows: anti-TCF12 (Santa Cruz, #sc-365980), anti-ASCL1 (Santa Cruz, #sc-390794) and IgG (Santa Cruz).

### Chromatin immunoprecipitation (ChIP)

Approximately 10 million cells were crosslinked with 1% formaldehyde (final concentration) for 10 min at room temperature, and the reaction was quenched with 250 mM glycine. The cell pellets were washed in PBS and then stored at -80°C. The pellets were lysed in lysis buffer I (50 mM HEPES-KOH (pH 7.5), 140 mM NaCl, 1 mM EDTA (pH 8.0), 10% glycerol, 0.5% NP-40, 0.25% Triton X-100, and protease inhibitor cocktail) for 10 min. After centrifugation, the supernatant was discarded, and the pellet was lysed in lysis buffer II (10 mM Tris-HCl (pH 8.0), 200 mM NaCl, 1 mM EDTA (pH 8.0), 0.5 mM EGTA (pH 8.0), and protease inhibitor cocktail) for 10 min. After centrifugation, the supernatant was discarded, and the pellet was washed and lysed in lysis buffer III (10 mM

Tris-HCl, 1 mM EDTA (pH 8.0), 0.1% SDS buffer, and protease inhibitor cocktail) and sonicated. Chromatin from GI-MEN cells was sheared with a Bioruptor Pico sonicator (Diagenode) operated at high power for 30 cycles of 30-s each with a 30-s interval between cycles to obtain an average DNA fragment size of 300 bp. Sheared chromatin was incubated with primary antibody-conjugated Dynabeads Protein A (Thermo Fisher Scientific) overnight in buffer (10 mM Tris-HCl, 100 mM NaCl, 1 mM EDTA (pH 8.0), 0.1% SDS buffer, 1% Triton X-, and protease inhibitor cocktail) prior to elution and reverse crosslinking at 65°C for 15 h. TE buffer was added to the DNA elution buffer prior to RNase treatment (0.45 mg/mL) at 37°C for 2 h and proteinase K treatment (0.3 mg/mL) at 55°C for 45 min. DNA was purified using a Zymo DNA purification kit. The final product was eluted in 25  $\mu$ L of nuclease-free water. The antibodies used for ChIP-PCR were as follows: anti-HA (Cell Signaling Technology, #3724) and IgG (Cell Signaling Technology, #2729). After purification of DNA, qPCR was performed using a Quant Studio 3 Real-Time PCR System (Thermo Fisher Scientific) with purified DNA, Power SYBR Green PCR Master Mix (Roche) and PCR primers specific for the genomic regions of interest. The PCR primer sequences are listed in [Table S7](#).

### Chromatin immunoprecipitation–sequencing (ChIP-seq)

For each ChIP reaction, 10  $\mu$ g of antibody was used per 20 million cells, and the procedures were carried out as described above. Anti-HA (Cell Signaling Technologies, #3724) and anti-H3K27ac (Abcam, #7429) antibodies were used. Library construction and Illumina HiSeq sequencing of  $\sim$ 25 M paired-end 150-bp reads were performed at BGI Biotech Solutions Co., Ltd. (Hong Kong, China). See the [data analysis](#) section for the details of the bioinformatics analysis.

### Hi-C chromatin immunoprecipitation (Hi-ChIP)

H3K27ac Hi-ChIP experiments were performed using an Arima-HiC<sup>+</sup> kit (Arima Genomics A160169), according to the manufacturer's protocols. A total of 10 million cells were fixed with freshly prepared 2% formaldehyde, and the reaction was quenched with Stop Solution 1. A total of 3 million cells were used per reaction. Cells were lysed with Hi-C lysis buffer. Nuclei were permeabilized with Conditioning Solution and quenched with Stop Solution 2. Chromatin was digested with Restriction Enzymes A1 and A2 for 1 h, subjected to biotin-dATP incorporation using Enzyme B, ligated using Enzyme C and sonicated using a Bioruptor Pico sonicator. For each reaction, the anti-H3K27ac antibody (in an amount based on the shearing yield and antibody ratio) was added to sheared chromatin and incubated at 4°C overnight with rotation. Chromatin-antibody complexes were captured with Protein-A magnetic beads. Then, the beads conjugated to the antibody and DNA were washed three times at room temperature. The washed ChIP sample beads were then resuspended in 100  $\mu$ L of DNA elution buffer. ChIP samples containing DNA fragments were then purified with a Zymo DNA purification kit (Zymo Research, Irvine, CA). The amount of DNA was quantified using a Qubit dsDNA HS Assay Kit (Thermo Fisher Scientific, Waltham, MA). Following the Hi-ChIP procedure, 10 ng of post-ChIP DNA per reaction was used for library preparation with a Swift Biosciences Accel-NGS 2S Plus DNA Library Kit (Arima Genomics A101020) for sequencing. See the [data analysis](#) section for the details of the bioinformatics analysis.

### Assay for transposase-accessible chromatin (ATAC)

Approximately 30,000 cells were washed twice using 50  $\mu$ L of cold 1  $\times$  PBS and centrifuged at 500  $\times$  g for 5 min. Cells were lysed using cold lysis buffer (10 mM Tris-HCl (pH 7.4), 10 mM NaCl, 3 mM MgCl<sub>2</sub> and 0.1% IGEPAL CA-630). Immediately after lysis, nuclei were centrifuged at 500  $\times$  g for 10 min using a refrigerated centrifuge. Immediately following nuclear preparation, the pellet was re-suspended in transposase reaction mix (25  $\mu$ L of 2  $\times$  TD buffer, 2.5  $\mu$ L of transposase (Illumina) and 22.5  $\mu$ L of nuclease-free water). The transposition reaction was carried out for 45 min at 37°C. Immediately after transposition, the sample was purified using a Zymo DNA purification kit. Following purification, we amplified library fragments using 1  $\times$  NEBNext PCR master mix and 1.25  $\mu$ M custom Nextera PCR primers 1 and 2 by PCR using the following thermal cycling conditions: 72°C for 5 min; 98°C for 30 s; 12 cycles at 98°C for 10 s and 63°C for 30 s; and a final extension step at 72°C for 1 min. The libraries were purified using a Zymo DNA purification kit. Illumina HiSeq sequencing of  $\sim$ 25 M paired-end 150-bp reads was performed at Genewiz (Suzhou, China). See the [data analysis](#) section for the details of the bioinformatics analysis.

### Cleavage under targets and release using nuclease (CUT&RUN)

CUT&RUN was performed using an EpiCypher kit (SKU: 14–1048). Approximately 0.5 million cells were used for each reaction. In brief, cells were attached to preactivated ConA beads for 10 min at room temperature. Then, 0.5  $\mu$ g of an antibody targeting the transcription factor or histone modification of interest as well as IgG were added to the reactions and incubated overnight at 4°C. The cells were incubated with pAG-MNase for 10 min at room temperature prior to activation by calcium chloride. The cells were then incubated at 4°C for 2 h prior to the addition of stop buffer. DNA was purified for library construction using an Illumina sequencing library kit. Illumina HiSeq sequencing of  $\sim$ 10 M paired-end 150-bp reads was performed at Genewiz (Suzhou, China). See the [data analysis](#) section for the details of the bioinformatics analysis.

## QUANTIFICATION AND STATISTICAL ANALYSIS

Details of the statistical analyses for the experiments are provided in the figure legends.

## Data analysis

### RNA-seq data analysis

RNA-seq reads were aligned to the hg19 human reference genome using STAR 2.5.2a with `outFilterMultimapNmax` set to 1. The total number of mapped reads was quantified using `featureCounts` version 2.0.1, and count tables were generated based on Ensembl hg19 gene annotation gtf files. Differential expression analysis was conducted using the Bioconductor package DESeq2 version 1.12.4. Gene expression in each neuroblastoma cell line was estimated in transcripts per million (TPM) using Kallisto software version 0.43.1. All RNA-Seq data were normalized using the Sleuth R package from the Pachter laboratory.<sup>44</sup> Selected gene expression data from the Sleuth normalized TPM file were used to generate a heatmap using the web-based heatmap tool `heatmapr`.<sup>45</sup>

### ATAC sequencing (ATAC-seq) analysis

Paired-end ATAC-seq reads were mapped to the bowtie2 human reference index (hg19) using Bowtie2 with `-k 10 --very-sensitive` parameters. Duplicates were removed from aligned ATAC-seq reads using the Picard `MarkDuplicates` with `--REMOVE_DUPLICATES true`. After duplication removal, non-uniquely aligned reads were filtered by removing reads with `MAPQ < 10` using `Samtools view -q 10`. MACS2 version 2.2.7.1 were used to call peaks with `--keep-dup = all -f BAMPE -p 1e-5 -B` and `--SPMR` parameters. The signal tracks were further compile using `MACS2 bdgcmp` with `-m subtract` mode to subtract the signal from its corresponding background values, further floored the signal to 0.1 and convert it to BigWig format by using the UCSC `bedGraphToBigWig` script. Signal tracks were uploaded and visualized in UCSC genome browser.

### ChIP-seq analysis

All ChIP-seq reads were mapped to the hg19 human reference genome using Bowtie2 with default parameters. Duplicates were removed from aligned ChIP-seq reads using the Picard `MarkDuplicate` package with `--REMOVE_DUPLICATES true`. ChIP-seq peaks were called with MACS2 software version 2.2.7.1 with `--keep-dup = 1 --SPMR -p 1e-9 -f BAM`. The output `bedGraph` data were normalized by subtracting the corresponding background values using `MACS2 bdgcmp -m subtract`. `BedGraph` signal were further floored to 0.1, then convert to `bigWig` format using UCSC `bedGraphToBigWig` tool. H3K27ac `broadPeaks` ( $P < 1e-9$ ) and ASCL1 `narrowPeaks` ( $P < 1e-9$ ) called by MACS2 were selected and filtered for promoter and non-promoter binding peaks based on `annotatePeaks` from the HOMER package. The cooccurrence heatmap and metagene plot were generated using `deepTools` version 3.1.2. Each signal matrix was calculated with the `deepTools computeMatrix` function using `bigwig` output files generated with UCSC `bedGraphToBigWig` for each ChIP-seq sample. The signal matrices were then used to generate a heatmap using the `deepTools plotHeatmap` package.<sup>46</sup>

### Hi-ChIP analysis

Hi-ChIP data were aligned and processed using HiC-Pro pipeline version 2.11.1, and the reads in the fastq files were aligned to the human reference genome (GRCh37/hg19) using Bowtie2 version 2.4.1. The restriction sites `GATC` and `GANTC` across the human genome were cut and utilized by HiC-Pro using the HiC-Pro Utilities Python script "digest genome". HiC-Pro configuration on ligation site were set to be `GATC` and `GANTC` optimize for ARIMA kit data. The aligned data were further processed using `hichipper` to call interactions. `Hichipper` version 2.7.9 was used to extract the valid interactions from the HiC-Pro data and to generate the `bedpe` interaction file. We utilized anchors from the peaks that were called in two sets of MACS2 `broadPeaks` data generated from the H3K27ac ChIP-Seq data using a p value cutoff  $< 1e-5$ . The peaks from both replicates were merged for use as anchors in the Hi-ChIP analysis.

### CUT&RUN analysis

CUT&RUN-seq data were preprocess and analyzed using `cutRunTools` pipeline.<sup>47</sup> This pipeline automated the preprocessing and alignment of CUT&RUN-seq data to hg19 genome. `CutRunTools` utilized MACS2 and SEACR software to call peaks using the default optimized cutoff for each CUT&RUN-seq data. The paired control data were further been utilized by the `cutRunTools step2` script to normalize the MACS2 and SEACR output peaks. Each `bedGraph` output has been further normalize by subtract the treatment file to the correspondence control file using `MACS2 bdgcmp` and floored the signal to 0.1 before convert to `bigWig` using UCSC `bedGraphToBigWig` tool.

### Principal component analysis (PCA)

PCA plots were generated using the online PCA tool available on the website <https://biit.cs.ut.ee/clustvis/>. Total of 4,133 genes that were differentially expressed between MES and ADRN neuroblastoma cell lines were used as variables. Differentially expressed genes were determined using public RNA-seq data.<sup>3</sup>

### Enrichr analysis

Gene enrichment analysis was performed using the online Enrichr tool available on the website <http://amp.pharm.mssm.edu/Enrichr/>.

### Motif analysis

Based on the ChIP-seq peaks called by MACS2, 500-bp sequences were retrieved from the peak summits. Enriched motifs were analyzed using the MEME-ChIP package from MEME SUITE with the *Homo sapiens* Comprehensive Model Collection (HOCOMOCO) v11 and the TRANscription FACtor (TRANSFAC) motif databases.